The Astrophysical Journal, 672:558–574, 2008 January 1

THE RISE AND FALL OF DEBRIS DISKS: MIPS OBSERVATIONS OF h AND χ PERSEI AND THE EVOLUTION OF MID-IR EMISSION FROM PLANET FORMATION

Thayne Currie,[1,2] Scott J. Kenyon,[1,3] Zoltan Balog,[4,5] George Rieke,[4] Ann Bragg,[3,6] and Benjamin Bromley[7]

Received 2007 July 9; accepted 2007 September 13

ABSTRACT

We describe *Spitzer* MIPS observations of the double cluster, h and χ Persei, covering a $\sim$0.6 deg^2 area surrounding the cores of both clusters. The data are combined with IRAC and 2MASS data to investigate $\sim$616 sources from 1.25–24 μm. We use the long-baseline $K_s - [24]$ color to identify two populations with IR excess indicative of circumstellar material: Be stars with 24 μm excess from optically thin free-free emission, and 17 fainter sources ($J \sim$ 14–15) with [24] excess consistent with a circumstellar disk. The frequency of IR excess for the fainter sources increases from 4.5 to 24 μm. The IR excess is likely due to debris from the planet formation process. The wavelength-dependent behavior is consistent with an inside-out clearing of circumstellar disks. A comparison of the 24 μm excess population in h and χ Per sources with results for other clusters shows that 24 μm emission from debris disks "rises" from 5 to 10 Myr, peaks at $\sim$10–15 Myr, and then "falls" from $\sim$15–20 Myr to 1 Gyr.

Subject headings: circumstellar matter — infrared: stars — open clusters and associations: individual (NGC 869, NGC 884) — planetary systems: formation — planetary systems: protoplanetary disks

Online material: machine-readable table

1. INTRODUCTION

Most 1–2 Myr old stars are surrounded by massive ($M_{\rm disk} \sim 0.01$–$0.1\ M_\star$) optically thick accretion disks of gas and dust. The disk produces near- to mid-infrared (IR) emission comparable in brightness to the stellar photosphere ($L_{\rm disk} \sim L_\star$) (e.g., Kenyon & Hartmann 1995; Hillenbrand 1998). The evolution of these "primordial" disks has been studied extensively (e.g., Haisch et al. 2001; Lada et al. 2006; Dahm & Hillenbrand 2007). By 5–10 Myr, primordial disks disappear and less massive ($M_{\rm disk} \lesssim 1\ M_\oplus$) gas-poor, optically thin "debris disks" with weaker emission ($L_{\rm disk} \lesssim 10^{-3}\ L_\star$) emerge (e.g., Hernandez et al. 2006). By $\sim$10–20 Myr, primordial disks are extremely rare: almost all disks are debris disks (Currie et al. 2007a, hereafter C07a; Gorlova et al. 2007; Sicilia-Aguilar et al. 2006).

Debris disks older than $\sim$20 Myr are well studied. Rieke et al. (2005, hereafter R05) showed that the 24 μm emission declines with time as t^{-1} (see also Kalas 1998; Habing et al. 2001; Decin et al. 2003). This decay agrees with expectations for the gradual depletion of the reservoir of small planetesimals. With fewer parent bodies to initiate the collisional cascades that yield the infrared-emitting dust, the infrared excesses drop systematically with time (Kenyon & Bromley 2002; Dominik & Decin 2003; R05; Wyatt et al. 2007b). R05 also found a large range in the amount of infrared excess emission at each age, even for very young systems. Wyatt et al. (2007b) demonstrate that the first-order cause of this range is probably the large variation in protostellar disk masses and hence in the mass available to form planetesimals.

Because the R05 sample and other studies of individual stars (e.g., Chen et al. 2005a) include few stars younger than 20 Myr, they do not probe the 5–20 Myr transitional period from primordial to debris disks well. This transition marks an important phase for planet formation and other physical processes in disks. Gas accretion onto most young stars ceases by $\approx$10 Myr (Sicilia-Aguilar et al. 2005). Planets acquire most of their mass by $\approx$5–20 Myr (Kenyon & Bromley 2006; Chambers 2001; Wetherill & Stewart 1993).

With an age of 13 ± 1 Myr and with over $\sim$5000 members (C07a), the double cluster, h and χ Persei ($d = 2.34$ kpc, $A_V \sim 1.62$; Slesnick et al. 2002; Bragg & Kenyon 2005), provides an ideal laboratory to study disk evolution during this critical age. Recent observations of h and χ Per with the *Spitzer Space Telescope* have demonstrated the utility of using the double cluster to investigate disk evolution after the primordial stage. C07a used 3.6–8 μm *Spitzer* data to show that disks last longer around less massive stars and at greater distances from the star. Currie et al. (2007b, hereafter C07b) analyzed a well-constrained subsample of h and χ Per sources and showed that at least some of the disk emission in them comes from warm dust in the terrestrial zones of disks as a by-product of terrestrial planet formation.

In this paper we use data obtained with the Multiband Imaging Photometer for *Spitzer* (MIPS) to extend the study of h and χ Per to 24 μm. This band allows us to search for high levels of mid-IR excess associated with cool dust that orbits in a disk at $\sim$2–50 AU from the central star. Our survey covers a region containing $\sim$600 intermediate- to high-mass cluster members. In § 2 we describe the MIPS observations, data reduction, and sample selection. We analyze the 24 μm photometry in § 3. The main results are (1) there are two IR-excess populations, Be stars with optically thin free-free emission and intermediate-mass stars likely harboring disks; (2) debris disk excesses are more common at 24 μm than at shorter wavelengths; and (3) there are several extreme disks similar to the nearby young debris disks around β Pic, HR 4796A, and 49 Cet. Finally, in § 4 we place h and χ Per in the context of

[1] Harvard-Smithsonian Center for Astrophysics, 60 Garden Street Cambridge, MA 02140; tcurrie@cfa.harvard.edu.
[2] Department of Physics and Astronomy, University of California, Los Angeles, CA, 90095.
[3] Visiting Astronomer, Kitt Peak National Observatory, National Optical Astronomy Observatory, which is operated by the Association of Universities for Research in Astronomy, Inc., under cooperative agreement with the National Science Foundation.
[4] Steward Observatory, University of Arizona, 933 North Cherry Avenue, Tucson, AZ 85721.
[5] On leave from the Department of Optics and Quantum Electronics, University of Szeged, H-6720, Szeged, Hungary.
[6] Department of Physics, Bowling Green State University, Bowling Green, OH.
[7] Department of Physics, University of Utah, 201 JFB, Salt Lake City, UT 84112.

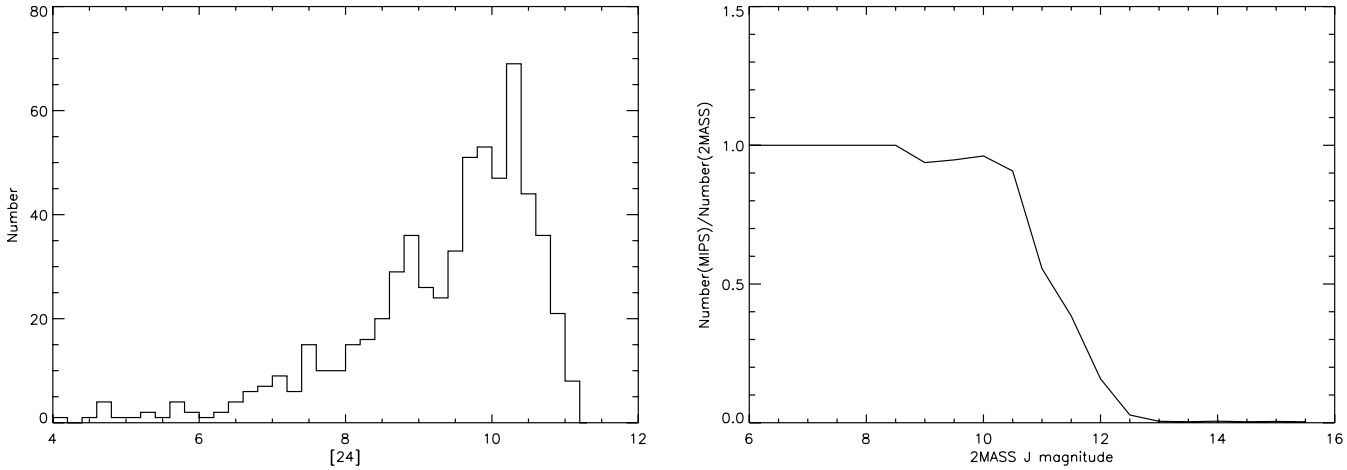

FIG. 1.—*Left*: Distribution of [24] magnitudes for sources detected at the 5 σ level with MIPS that have 2MASS/IRAC detections. The number counts peak at [24] $\sim$ 10.5. *Right*: The completeness profile as a function of 2MASS *J* magnitude. Through $J = 10.5$, $\gtrsim$90% of all the 2MASS sources are detected with MIPS. Only about half of the 2MASS sources between $J = 10.5$–11 are detected with MIPS.

results for other open clusters/associations with optically thin debris disk candidates. The flux from debris disks rises from $\sim$5 Myr (when they first emerge), peaks at $\sim$10–15 Myr, and then falls as t^{-1} as described by R05. We conclude with a summary of our findings and discuss future observations that may place even stronger constraints on debris disk evolution by accounting for wide range of IR excesses at 10–15 Myr.

2. OBSERVATIONS

2.1. *MIPS and Ground-based Spectroscopic Data*

We acquired MIPS 24 μm data using 80 s exposures in scan mode, covering two 0.3 deg^2 regions centered on the two clusters. The frames were processed using the MIPS Data Analysis Tool (Gordon et al. 2005). PSF fitting in the IRAF/DAOPHOT package was used to obtain photometry using a 7.3 Jy zero point for the 24 μm magnitude scale. The typical errors for the MIPS sources are 0.2 mag ($\sim$5 σ) at a 24 μm magnitude of [24] $\sim$ 10.5–11. The number counts for the MIPS data peak at [24] $\sim$ 10.5 and decline to zero by [24] $\sim$ 11.5 (Fig. 1*a*). We detect 2493 potential h and χ Per sources.

We combined the MIPS photometry with the 2MASS/IRAC catalog of h and χ Persei from C07a. To minimize potential contamination of stellar sources by background PAH-emission galaxies and AGNs, we used a small 1.25″ matching radius (about half of a MIPS pixel; r_M) to merge the 2MASS/IRAC and the MIPS catalogs. Although the MIPS beam is 6″ in diameter, the instrument delivers positions good to 1″ even for faint sources in crowded fields (Bai et al. 2007). This procedure yielded 616 sources ($N_{\rm MIPS}$) with high-quality 1–24 μm photometry. Table 1 shows the 2MASS/IRAC + MIPS catalog. Optical *UBV* photometry from Slesnick et al. (2002) is included where available.

To [24] = 10.5, the probability of chance alignments between distant PAH-emission galaxies/AGNs and our sources is low. Using the galaxy number counts from Papovich et al. (2004), $N_G \sim 3.5 \times 10^6$ sr^{-1}, we derive a probability of $\sim$24.8% that one of our 616 sources is contaminated [$\pi r_M^2 \times N_G \times N_{\rm MIPS}/(3282.8 \times 3600^2)$]. The likelihood that many of our sources are contaminated is then much smaller.

To estimate the completeness of the MIPS sample, we compare the fraction of *J*-band sources detected with MIPS within either cluster. Figure 1*b* shows that $\gtrsim$90% of the 2MASS sources brighter than $J = 10.5$ are also detected in MIPS. The completeness falls to $\sim$50% by $J = 11$ and to $\sim$10% by $J = 12$. The dip at $J \sim 8$–9 occurs because many sources in this range are near the cluster centers, where the high density of even brighter sources ($J \sim 6$–8) masks the presence of fainter objects.

To provide additional constraints on the 24 μm excess sources, we also obtained Hectospec (Fabricant et al. 2005) and FAST (Fabricant et al. 1998) spectra of selected MIPS sources on the 6.5 m MMT and 1.5 m Tillinghast Telescope at F. L. Whipple Observatory during 2006 September–November. Spectra for bright sources ($J \leq 13$) were also cross referenced with the FAST archive. The FAST spectroscopy, described in detail by Bragg & Kenyon (2002), typically had $\sim$10 minute integrations using a 300 g mm^{-1} grating blazed at 4750 Å and a 3″ slit. These spectra cover 3700–7500 Å at 6 Å resolution. The typical signal-to-noise ratios were $\gtrsim$25–30 at 4000 Å. For each Hectospec source, we took three, 10 minute exposures using the 270 mm^{-1} grating. This configuration yields spectra at 4000–9000 Å with 3 Å

TABLE 1
MIPS SOURCES WITH 2MASS/IRAC COUNTERPARTS IN h AND χ PERSEI

α	δ	V	$B-V$	$U-B$	J	H	K_s	[3.6]	[4.5]	[5.8]	[8]	**[24]**	σ([3.6])	σ([4.5])	σ([5.8])	σ([8])	σ**([24])**
35.4810.....	57.2429	6.480	0.502	−0.050	5.08	4.86	4.77	8.39	...	4.73	4.52	4.14	0.01	0.00	0.00	0.00	0.03
34.8081.....	57.1693	6.700	0.503	−0.428	5.53	5.37	5.31	...	...	5.30	5.07	4.64	0.00	0.00	0.00	0.00	0.03
34.7685.....	57.1355	6.567	0.452	−0.346	5.56	5.43	5.29	8.18	7.05	5.25	5.17	4.68	0.01	0.00	0.00	0.00	0.00
35.7517.....	57.3870	6.977	0.707	−0.249	5.59	5.38	5.26	8.31	...	5.16	5.04	4.73	0.04	0.00	0.00	0.00	0.03
34.2155.....	57.0552	...	...	...	5.78	5.71	5.61	...	...	...	...	5.00	0.00	0.00	...	...	0.03

NOTES.—First five entries in our photometry catalog from MIPS, 2MASS and IRAC. We also include optical *UBV* photometry from Slesnick et al. (2002). Errors in the 2MASS *JHK*$_s$ filters are $\lesssim$0.05 for sources except the $\sim$21 fainter ($J \sim 14$–15) sources. Table 1 is also available in machine-readable form in the electronic edition of the *Astrophysical Journal*.

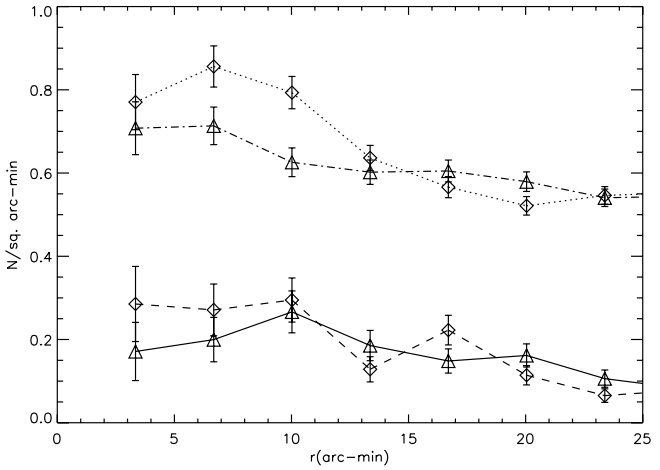

FIG. 2.—Number density distribution of MIPS-detected sources as a function of distance from h Persei (*diamonds, dashed line*) and χ Persei (*triangles, solid line*). The error bars are based on Poisson statistics. The number counts decline through $\sim$20′ away from both cluster centers, although because of the small area coverage it is unclear exactly where the true background lies. For reference, we show the number density of 2MASS sources ($J \leq 15.5$) as a function of distance away from h Persei (*diamonds, dotted line*) and χ Persei (*triangles, dot-dashed line*) divided by 5. The peak number density of MIPS sources is about an order of magnitude smaller than for 2MASS *J* band as found by C07a.

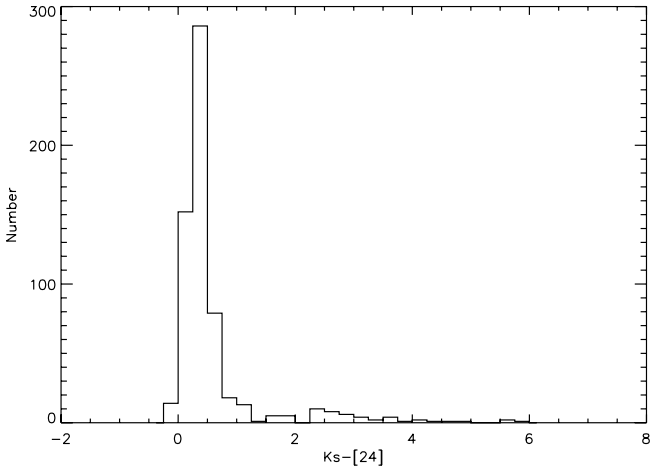

FIG. 3.—Distribution of $K_s - [24]$ colors for the 2MASS/MIPS detections. The distribution is peaked at $K_s - [24] \sim 0$–0.5 and has a long positive tail stretching to $K_s - [24] \sim 6$.

resolution. The data were processed using standard FAST and Hectospec reduction pipelines (e.g., Fabricant et al. 2005).

We acquired additional spectra of h and χ Per sources with the Hydra multifiber spectrograph (Barden et al. 1993) on the WIYN 3.5 m telescope at the Kitt Peak National Observatory. Hydra spectra were obtained during two observing runs in 2000 November and 2001 October and include stars brighter than $V = 17.0$. We used the 400 g mm^{-1} setting blazed at 42°, with a resolution of 7 Å and a coverage of 3600–6700 Å. The standard IRAF task `dohydra` was used to reduce the spectra. These spectra had high signal-to-noise ratios with $\gtrsim$1000 counts over most of the wavelength coverage.

2.2. *Spatial Distribution of MIPS Sources*

To investigate the spatial distribution of the MIPS sources and the likelihood that they are cluster members, we compare the projected sky surface densities derived from MIPS and 2MASS. C07a showed that $\sim$47% of stars within 15′ of the cluster centers are cluster members. Between 15′ and 25′, $\sim$40% of the 2MASS sources are in a halo population with roughly the same age as bona fide cluster stars. Because the MIPS coverage is complete only out to $\sim$15′ away from each cluster center, we cannot identify MIPS sources with this halo population. We compare the spatial distribution of MIPS sources to those in 2MASS from C07a by calculating the number density of sources in 5′ wide half-annuli facing away from the midpoint of the two clusters.

Through 15′ away from either cluster center, the number counts of sources detected with both MIPS and 2MASS fall off about as steeply or slightly more steeply than the counts for 2MASS alone from C07a (Fig. 2). Near the center of the clusters the density of MIPS sources is $\sim$0.4 arcmin^{-2}, or about an order of magnitude lower than from 2MASS. For h Persei and χ Persei, respectively, this density falls off by 4% and 25% from 0′–5′ to 5′–10′ away from the cluster centers and 22%–41% from 0′–5′ to 10′–15′ away from the centers. The low counts through 5′ and more shallow drop in number density for χ Persei is due to crowding in the inner $\sim$1′–2′ of the χ Persei core; the slope of the MIPS number density in χ Persei shown in Figure 2 is most likely a lower limit. In contrast, the number counts for the 2MASS data from C07a fall off by 10% (20%) and 30% (32%) for h (χ) Persei over the same 5′ intervals (the values in Fig. 2 are slightly different due to the larger annuli used here). The MIPS source counts appear to be about as centrally concentrated as the 2MASS counts.

2.3. *General Nature of the* 24 μm *Sources*

Figure 3 shows the histogram of $K_s - [24]$ colors for the MIPS detections with 2MASS counterparts. The histogram has a main peak at $K_s - [24] \sim 0$–1 and two groups with $K_s - [24] \sim 1$–2 and $K_s - [24] \sim 2$–6. The sources with very red $K_s - [24]$ colors ($\geq$2) are in two main groups (Fig. 4). A bright group of very red sources has $K_s \sim 9$–11; a fainter population of red sources stretches from $K_s \sim 13.5$–15. A population of 13 Myr old stars in h and χ Per with spectral types later than B9 ($M \leq 3.0\ M_\odot$) should have *J*, K_s magnitudes $\gtrsim$13.3 (Siess et al. 2000). Thus, some of these fainter sources with red $K_s - [24]$ colors are possibly pre–main-sequence stars.

Some of the sources are very faint in the near-infrared. To examine the nature of the MIPS sources without *J* counterparts, we first compared the MIPS mosaic and the 2MASS *J* mosaic by

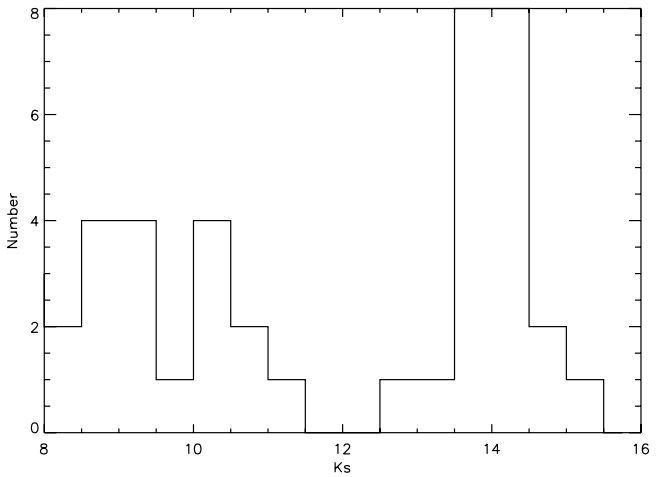

FIG. 4.—Distribution of K_s magnitudes with strong IR excess in the MIPS bands ($K_s - [24] \geq 2$). There appear to be two populations of strong MIPS excess sources: a bright distribution from $K_s = 9$–11 and a faint distribution from $K_s = 13.5$–15.

eye. Many sources appear scattered throughout the MIPS mosaic but do not appear in 2MASS, even at very high contrast. These sources are likely cluster stars with $J \gtrsim 16$–17 and very red $J - [24]$ colors or background galaxies with negligible near-IR emission. Using the number density of galaxies in the MIPS 24 μm filter from Papovich et al. (2004), we expect $\gtrsim$600–700 galaxies in the 0.6 deg^{-2} coverage area brighter than $[24] \sim 10.5$. Thus, many of the sources without 2MASS counterparts are likely not h and χ Per members. From the C07a survey, there are $\sim$4700 stars with $J \sim 10$–15.5 within either cluster or the surrounding halo population of comparable age. For a reasonable IMF (e.g., Miller & Scalo 1979), we expect $\sim$2800 ($\sim$8900) cluster/halo stars with $J \sim$ 16-17 (17–18). If $\sim$10%–20% of these stars have large 24 μm excesses, as predicted from an extrapolation of the C07a results to fainter J magnitudes, we expect 1170–2340 cluster/halo stars with MIPS detections and no 2MASS counterparts. Together with the 600–700 background galaxies, this population yields the observed number of MIPS detections without 2MASS counterparts.

3. A [24] IR EXCESS POPULATION IN h AND χ PERSEI

3.1. *Groups in the J, J − H Color-Magnitude Diagram*

To identify the nature of the 24 μm emission in sources with red $K_s - [24]$ colors in Figure 2, we refer to previous MIPS observations of very "red" sources and consider possible contaminants. MIPS observations of the Pleiades (Gorlova et al. 2006) guide our analysis of $K_s - [24]$ colors for IR excess disk/envelope sources. While the stellar density in h and χ Per is larger than in the Pleiades, other possible contaminants are less important. The level of galactic cirrus for h and χ Persei is much lower than for the Pleiades: 17–27 MJy sr^{-1} versus 36–63 MJy sr^{-1}. Gorlova et al. found that disk-bearing candidate sources have dereddened $K_s - [24]$ colors $\gtrsim$0.25. Because h and χ Persei has a low, uniform extinction of $A_V \sim 1.62, E(B - V) \sim 0.52$ (Bragg & Kenyon 2005), we convert the dereddened $K_s - [24]$ excess criterion into a reddened $K_s - [24]$ criterion using the reddening laws from Indebetouw et al. (2005) and Mathis (1990). For $A_V \sim 1.62$, 24 μm excess sources should have $K_s - [24] \gtrsim 0.45$. Because the MIPS data have $\sigma \lesssim 0.2$, we round this limit up to $K_s - [24] \gtrsim 0.65$.

Figure 5 shows the distribution of sources with and without $K_s - [24]$ excess in J/J−H color-magnitude space. The IR excess population is clustered into two main groups. Asterisks (*diamonds*) denote sources brighter (fainter) than $J = 13$. Larger asterisks/diamonds correspond to sources with $K_s - [24] \geq 2$, while smaller asterisks identify sources with $K_s - [24] = 0.65$–2 and $J \leq 13$.

The excess sources with $J \leq 13$ typically have J−H colors $\sim$0.2 mag redder than a typical stellar photosphere. Many sources with weak excess lie well off the 14 Myr isochrone and may be consistent with foreground M stars or supergiants. About 17 out of 21 stars with 24 μm excess fainter than $J = 13$ fall along the 14 Myr isochrone with $J \approx 14$–15. At 14 Myr and a distance of 2.4 kpc, this J magnitude range corresponds to stars with masses $\sim$2.2–1.4 $M_\odot$ (B9/A0–G2) stars (Siess et al. 2000). We inspected each faint excess source on the MIPS mosaic for extended emission (indicative of galaxies) or "excess" due to source confusion/crowding. We found no evidence issues such as large extended emission or source confusion that could compromise the photometry of any of the faint excess sources.

3.2. *Two Populations of IR-Excess Sources: Be Stars with Circumstellar Envelopes and Faint Pre–Main-Sequence Stars with Disks*

There are three main possibilities for the source of 24 μm excess emission around h and χ Per stars. Red giants or supergiants not associated with the clusters or the halo produce IR excesses in massive stellar winds, and should have $J - H \gtrsim 0.5$. Two such stars have large 24 μm excesses and are not considered further. Be stars in the clusters/halo population have IR excesses from optically thin free-free emission and should have $J \lesssim 13$–13.5 and $J - H \lesssim 0.4$. Many potential Be stars have $K_s - [24] \sim 2$ (Fig. 5; *large asterisks*) and clearly are an important part of the cluster population. Aside from Be stars, circumstellar disks around lower mass cluster/halo stars can produce excess emission. Figure 5 shows a significant population of fainter stars (all with $J \gtrsim 13.5$) on the 14 Myr isochrone with large $K_s - [24]$ excesses. To identify the nature of the 24 μm excess sources, we analyze the near-IR colors and selected spectra of the excess population. We begin with Be star candidates and then discuss the fainter population.

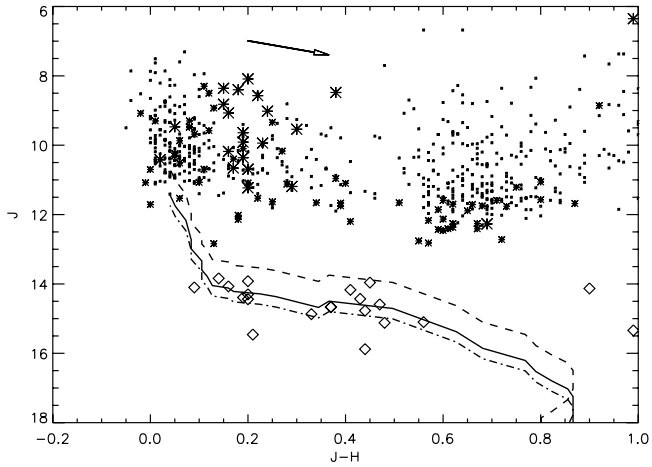

FIG. 5.—Distribution of photospheric (*small squares*), marginal [24] excess (small asterisks for sources brighter than $J = 13$) and strong [24] excess (large asterisks for $J \leq 13$; diamonds for $J \geq 13$) sources. "Marginal" and "strong" excesses are defined as sources with $K_s - [24] = 0.65$–2 and $K_s - [24] \geq 2$, respectively. The 14 Myr Siess et al. (2000) isochrone (*solid line*), reddened to $A_V = 1.62$ (reddening vector shown as arrow), is plotted with a 0.3 mag lower bound (*dot-dashed line*) for photometric errors and a 0.75 mag upper bound (*dashed line*) for binarity. There are two sources at $J \sim 14.66$, $J - H \sim 0.36$ that are not distinguishable on this plot.

Be stars are massive and are evolving off the main sequence (McSwain & Gies 2005). The IR-excess emission from Be stars arises from an optically thin, flattened, circumstellar shell of ionized gas ejected from the star (Woolf et al. 1970; Dachs et al. 1988). We find 57 candidates—$J \lesssim 13.5$ and $J - H \leq 0.4$—with 24 μm excess ($K_s - [24] \gtrsim 0.65$). Twenty of these stars have been previously identified as Be stars by Bragg & Kenyon (2002), all with Oosterhoff (1937) numbers, and have spectral types from Strom & Wolff (2005) and Bragg & Kenyon (2002). Table 2 lists the properties of these 57 candidates.

We can estimate the ratio of Be stars to B stars over a narrow range of spectral types (earlier than B4). In our MIPS survey, there are $\sim$175 stars that are likely B-type stars ($J = 8$–13.5; $J - H \leq 0.2$) without excess. All of these stars are probably earlier than B4 based on their 2MASS J-band photometry ($J \lesssim 11.75$). There are 57 Be star candidates with 24 μm excess ($K_s - [24] \gtrsim 0.65$): 51 of these stars probably have spectral types earlier than B4 based on their J-band photometry. The ratio of Be star candidates to main-sequence B-type stars earlier than B4 in the MIPS survey is then $\sim$0.29. This estimate is larger than the ratio derived from optical and near-IR data ($\sim$0.14; Bragg & Kenyon 2002). We explored this difference as follows.

First, we analyze the Be star candidate population in high-density regions close to the cluster centers where spectroscopic

TABLE 2

Be Stars/Candidates and Selected Evolved Stars with 24 μm Excess in h and χ Persei

Number	Oosterhoff Number	Spectral Type	α	δ	V	J	H	K_s	[8]	[24]
1	2589	Be	35.7229	57.2452	7.48	5.89	5.62	5.47	4.92	4.50
2	847	B1.5Ie	34.6997	57.0673	9.13	8.30	8.19	8.10	7.61	6.42
3	1261	B3 Ve	34.8605	57.0784	9.56	8.40	8.22	7.87	6.30	4.93
4	2284	B0e	35.5268	57.0903	9.68	8.48	8.10	7.55	5.65	4.76
5	2402	B1e	35.5947	57.2847	9.64	8.50	8.38	8.33	7.02	6.67
6	2088	B1 IIIe	35.4308	57.1258	9.49	8.82	8.67	8.58	8.43	6.30
7	1161	B1 Ve	34.8069	57.1288	10.22	9.07	8.91	8.68	7.60	6.42
8	846	B1e	34.7015	57.2403	9.98	9.08	9.10	9.06	8.42	7.49
9	517	B3e	34.5629	57.1711	14.59	9.30	9.22	9.08	8.53	7.43
10	2165	B1 Ve	35.4705	57.1664	10.15	9.47	9.42	9.41	7.81	6.76
11	2566	B1e	35.7004	57.2002	10.63	9.58	9.46	9.30	9.14	8.16
12	1282	09e	34.8701	57.1179	11.00	9.64	9.45	9.21	7.79	6.85
13	2649	B2e	35.7674	57.1275	10.64	9.68	9.59	9.49	9.07	8.32
14	2242	B3e	35.5103	57.1557	10.96	10.10	9.91	9.67	9.05	7.85
15	1438	B2e	34.9493	57.1110	11.20	10.18	10.02	9.87	8.47	7.62
16	1278	B2e	34.8703	57.1901	11.59	10.66	10.49	10.29	9.50	8.00
17	2091	B2e	35.4353	57.1812	11.72	10.69	10.49	10.30	9.17	7.86
18	1114	B3e	34.7859	57.0636	12.40	11.19	10.90	10.69	9.48	7.88
19	1977	B2e	35.3538	57.1979	12.28	11.23	11.03	10.82	9.66	8.21
20	563	Be	34.5822	57.1462	12.27	11.53	11.47	11.45	11.30	10.38
21	99	B3 I	34.8081	57.1693	6.7	5.53	5.37	5.31	5.07	4.64
22	99	99	34.2405	57.1302	99.00	8.09	7.89	7.52	6.32	5.24
23	99	B1 Ie	35.4617	57.3866	9.27	8.36	8.21	8.08	99.00	5.30
24	99	99	35.3253	57.3062	9.74	8.57	8.35	8.11	6.97	5.56
25	99	99	35.1627	57.3119	9.64	8.93	8.80	8.67	8.83	7.45
26	99	99	35.8538	57.3177	10.60	9.02	8.78	8.53	7.33	5.95
27	99	99	34.5765	56.8506	9.70	9.30	9.29	9.27	9.33	8.30
28	99	99	35.8877	57.0757	10.45	9.34	9.09	8.81	8.62	6.86
29	99	99	33.9481	57.4207	99.00	9.47	9.39	9.21	99.00	7.44
30	99	99	34.1349	57.5337	99.00	9.48	9.40	9.31	99.00	8.39
31	99	99	35.6957	56.9683	10.70	9.54	9.24	8.91	7.72	6.29
32	99	99	35.7228	56.7871	10.61	9.87	9.81	9.75	9.82	9.08
33	99	99	35.8673	57.3905	11.19	9.91	9.72	9.48	8.34	6.97
34	99	99	36.1358	57.0125	99.00	9.94	9.71	9.40	99.00	6.88
35	99	99	35.2199	57.2244	11.62	10.17	9.90	9.62	9.51	7.70
36	99	A2	35.6384	57.0416	10.79	10.24	10.19	10.12	10.08	9.17
37	99	99	35.9502	56.7838	11.27	10.31	10.26	10.22	10.14	9.52
38	99	99	36.1420	56.8837	99.00	10.36	10.17	10.15	99.00	7.30
39	99	99	36.0424	57.3254	11.85	10.40	10.23	10.21	99.00	8.97
40	99	99	35.0563	56.7401	99.00	10.42	10.40	10.38	8.64	7.81
41	99	99	34.4142	57.0958	11.25	10.51	10.45	10.40	10.33	9.16
42	99	99	34.9078	56.7302	11.40	10.69	10.58	10.56	10.57	9.90
43	99	99	34.3799	56.9881	11.27	10.70	10.70	10.65	10.65	9.96
44	99	99	33.9740	57.1986	99.00	10.96	10.58	10.47	99.00	9.71
45	99	99	35.0169	57.0555	11.91	11.07	10.97	10.92	10.90	10.07
46	99	99	34.9094	56.8205	11.62	11.08	11.09	11.06	11.11	10.08
47	99	99	35.8650	57.3698	12.17	11.09	10.89	10.85	10.64	9.61
48	99	F7	35.7907	57.1709	12.39	11.12	10.84	10.80	10.77	10.03
49	99	99	34.5332	57.3827	13.13	11.53	11.31	11.17	11.11	10.47
50	99	99	36.3024	57.0817	99.00	11.63	11.38	11.30	99.00	10.54
51	99	G2	34.6765	57.2288	13.18	11.66	11.32	11.17	11.15	10.45
52	99	G1	35.4931	57.1820	13.26	11.67	11.28	11.18	11.10	10.49
53	99	B4 V	34.5567	57.2121	12.46	11.71	11.71	11.62	11.68	10.57
54	99	99	34.4228	57.4477	13.34	11.75	11.36	11.34	11.29	10.68
55	99	99	34.7373	57.4550	13.31	12.02	11.84	11.79	11.69	10.72
56	99	99	35.5442	57.5230	13.40	12.14	11.96	11.87	11.59	10.30
57	99	99	35.3152	57.2595	13.91	12.84	12.71	12.59	12.32	10.63

Notes.—List of Be stars, Be star candidates, and selected evolved stars with 24 μm excess emission in h and χ Persei. We include the Oosterhoff (1937) number, spectral type, luminosity class (I-supergiant, III-giant, V-dwarf), and V magnitude where available. All sources with the "e" designation in spectral type are Be stars. The first twenty entries are confirmed Be stars from Bragg and Kenyon (2002) and have Oosterhoff numbers. Slesnick et al. (2002) identify an additional Be star in lower density regions surrounding the center of h and χ Per (source number 23). All the other stars (referred to as "candidate Be stars" in the text) are either supergiants, foreground stars, or B-type cluster members from either Slesnick et al. (source 21) or archived spectroscopic data from FAST (the five other sources).

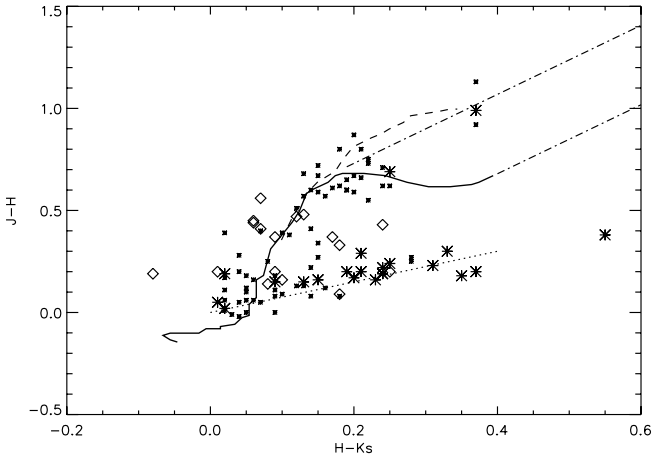

FIG. 6.—Distribution of 24 μm excess sources in observed $J - H/H - K_s$ color-color space. The symbols are the same as in the previous figure. The reddening band is overplotted as two straight dash-dotted lines. Only the faint sources lying along the 14 Myr isochrone are included. The bright sources with $K_s \geq 2$ follow a clear Be star locus (*dotted line*) from zero color to $J - H = 0.2$, $H - K_s = 0.3$; bright sources with weaker excess ($K_s - [24] \sim 0.65$–2) appear either along the Be star locus or close to the giant locus (*curved dashed line*). The faint excess sources appear to be evenly distributed across the photospheric track (*solid line*). The IR-excess population is probably comprised of two main groups: bright Be stars with optically thin free-free emission and fainter ($J \leq 13.5$) pre–main-sequence A–F stars that likely harbor protoplanetary disks.

data on bright stars in h and χ Per is complete. Our candidates were cross correlated with spectroscopically identified Be stars from Bragg & Kenyon within 5′ of the cluster centers. Ten known Be stars and two candidate stars from the MIPS survey are in this region. These two candidate stars with 24 μm excesses are not Be stars. One is a fifth-magnitude B3 supergiant cluster member identified by Slesnick et al. (2002), and the other is a G1 star, lying well off the isochrone with $J = 11.67$ and $J - H = 0.39$.

Because our spectroscopic sample of Be stars is spatially limited, we turn to near-IR colors from 2MASS to investigate the nature of the bright MIPS excess sources. Dougherty et al. (1991, 1994) showed that Be stars follow a distinct locus in JHK_s colors. This locus is characteristic of free-free emission from optically thin ionized gas and is well separated from main-sequence colors and the near-IR colors produced by warm dust. Thus, the $J - H/H - K_s$ color-color diagram (Fig. 6) provides a clear way to distinguish Be stars from lower mass stars with circumstellar dust emission. From Figure 6, it is clear that the bright sources with $K_s - [24] \geq 2$ follow a locus (*dotted line*) in $J - H/H - K_s$ from (0, 0) to (0.3, 0.4), a range consistent with known Be star colors (Dougherty et al. 1991, 1994). The bright sources with weaker excess (*small asterisks*) also appear to lie along the Be star locus or are clumped close to the red giant locus at $J - H \sim 0.6$–0.8, $H - K_s \sim 0.2$–0.3. The observed distribution of IR colors suggests ≈15 Be stars and ≈25 giants/supergiants. If this ratio is confirmed by optical spectroscopy, then the fraction of Be stars among all B-type stars is similar to the 14% derived by Bragg & Kenyon (2002).

Finally, we search the FAST archive at the Telescope Data Center at the Smithsonian Astrophysical Observatory and the Slesnick et al. catalog for additional spectra of the 35 Be star candidates in lower density regions. The FAST archive contains additional data for four candidates; we find one additional source from Slesnick et al. The Slesnick et al. source is a confirmed Be star (B1 Ie). The FAST sources contain an A2, F7, G2, and B4 star. The first three of these are bright and likely either foreground or giants associated with the halo population of h and χ Per. Thus, the spectra support our conclusion from the color-color diagram (Fig. 6) that many of the candidate Be stars are not true identifications. If none of the remaining candidate stars are true Be stars, then the ratio of Be stars to B stars is ∼0.12, close to the Bragg & Kenyon value.

Interestingly, the B4 star identified by Bragg & Kenyon (2002), has 24 μm excess *and* has a J magnitude and $J - H$ colors marginally consistent with an early B star in h and χ Per. The $K_s - [24]$ excess for this source is ∼1.05, although unlike Be stars it lacks clear IR excess at JHK_s and in the IRAC bands. We show its spectrum compared with that of a known Be star (Oosterhoff number 517) in Figure 7. This star is the earliest, highest mass star+circumstellar disk source known so far in h and χ Per.

Based on their near-IR colors and optical spectra, the faint excess sources in our survey are clearly distinguishable from Be stars. The near-IR colors of the faint excess sources are evenly distributed between $J - H = 0.1$–0.6 and $H - K_s = 0$–0.2 (Fig. 6, *diamonds*). The lack of very red $H - K_s$ colors for a typical faint excess source is consistent with a lack of warm ($T \sim 1000$ K) circumstellar envelope emission. Nearly all (17/21) faint sources are photometrically consistent with h and χ Per membership, although high-quality spectroscopic data are currently limited to eight sources (two from Hydra, six from Hectospec). Figure 8 shows the spectra. Seven of the eight faint excess sources have

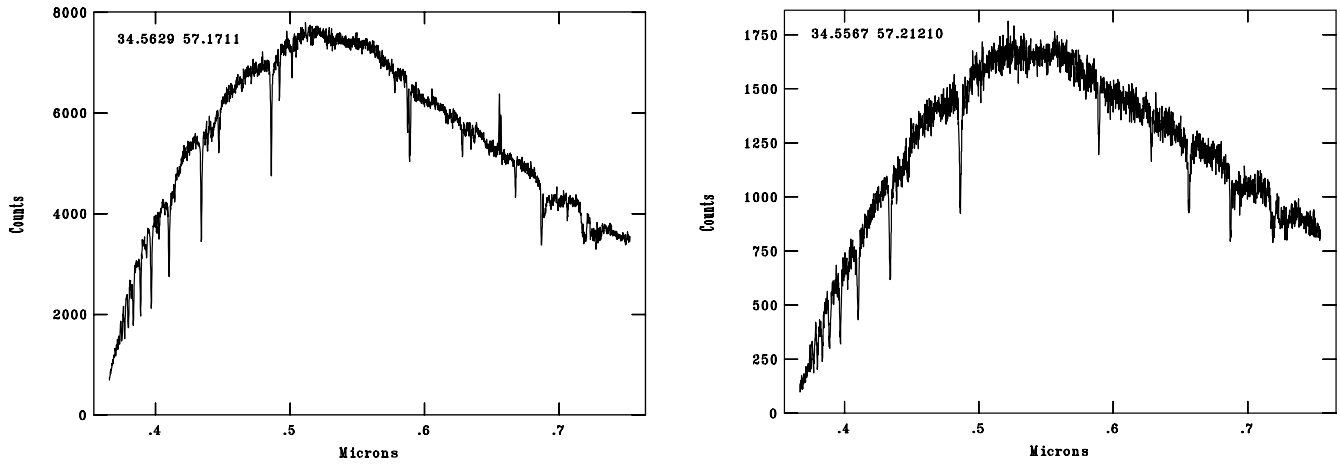

FIG. 7.—Sample spectra of bright ($J \leq 13$) 24 μm excess sources in the MIPS field. The source on the left was identified as a Be star from Bragg & Kenyon (2002) and has IR-excess emission from a circumstellar envelope. The source on the right has a spectral type of B4 and appears to be consistent with cluster membership.

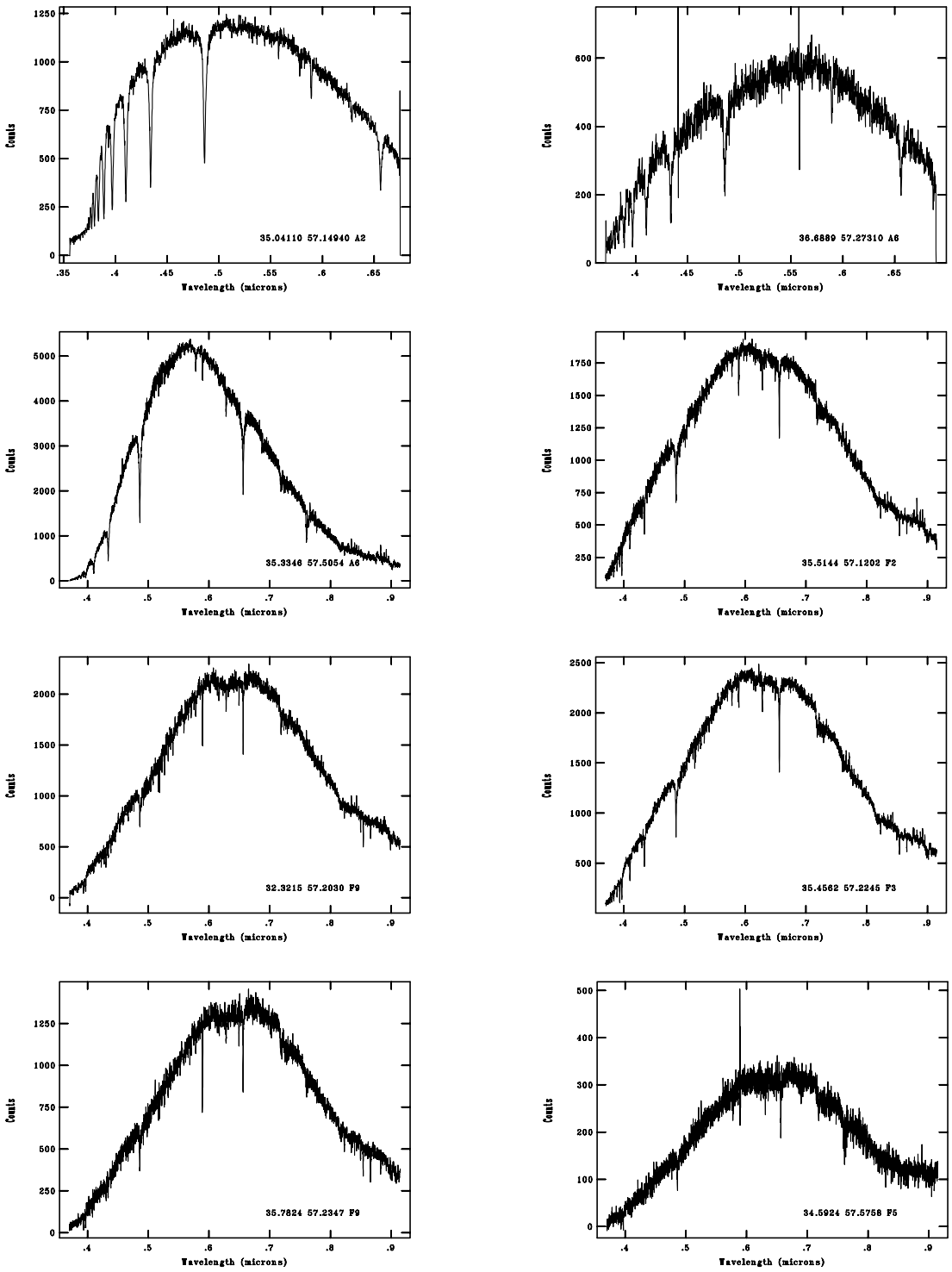

FIG. 8.—Spectra for eight faint ($J \geq 13$) stars with 24 μm excess observed with Hydra (*top two panels*) and Hectospec (*bottom six panels*). The coordinates and spectral types for each source are listed on the top of each plot. The A6 star observed with Hydra has some image artifacts (spikes in count level well above the continuum level) at ~0.44 and 0.56 Å due to bad sky subtraction, although this did not impact the spectral type determination as we use other spectral indices that were not contaminated. The F5 star lies about 1 mag fainter than the 14 Myr isochrone for h and χ Persei ($J \sim 15.9$) and is thus both photometrically and spectroscopically inconsistent with cluster membership. The other stars are both photometrically and spectroscopically consistent with being ~13–14 Myr old at a distance of 2.34 kpc. Thus, 7 of the 17 faint MIPS-excess sources lying on the $J/J - H$ isochrone for h and χ Per are spectroscopically confirmed members.

spectra consistent with h and χ Per membership. The one nonmember source in Figure 8 is an F5 star with $J = 15.9$, beyond the 2MASS completeness limit and below the isochrone by ~1.0 mag, and thus is one of the four faint sources that is also photometrically inconsistent with cluster membership. The spectral types for the seven sources consistent with cluster membership range from A2 to F9. None show strong Hα emission which is a signature of accretion (e.g., White & Basri 2003) and thus a reservoir of circumstellar gas. These stars are therefore very similar to the nearby young (8–12 Myr old) debris disks β Pic, HR 4796A, and 49 Cet in that they have comparable spectral types, have 24 μm excess, and lack any signatures of gas accretion.

TABLE 3
Observed Properties of Faint MIPS Excess Sources in h and χ Persei Consistent with Membership

α	δ	Spectral Type	J	K_s	$K_s - [4.5]$	$K_s - [5.8]$	$K_s - [8]$	$K_s - [24]$
35.0411.....	57.1494	A2	13.84	13.62	0.16	0.27	−0.26	2.81
35.4339.....	57.0355	A2?	13.92	13.71	0.17	0.21	0.21	3.14
36.0559.....	57.1190	A2?	13.96	13.45	99	99	99	2.36
35.3783.....	57.2056	A2?	14.07	13.81	0.22	0.31	0.24	3.02
35.1178.....	57.2625	A3?	14.10	13.83	0.15	0.18	0.06	3.17
34.7041.....	56.9259	A4?	14.17	13.69	0.18	0.09	0.19	4.38
36.2329.....	57.0037	A6?	14.30	14.01	99	99	99	3.86
35.3346.....	57.5054	A6	14.39	14.28	0.35	−0.27	99	3.53
36.0860.....	57.0493	A6?	14.43	13.76	99	99	99	4.18
34.6889.....	57.2731	A6	14.44	13.99	0.13	0.33	0.43	3.67
34.8108.....	57.4067	F2?	14.59	14.00	0.21	0.26	0.26	3.67
35.5144.....	57.1202	F2	14.66	14.20	99	99	99	3.16
35.3215.....	57.2030	F9	14.67	14.13	0.25	0.33	0.47	3.26
35.1171.....	57.2662	F9?	14.77	14.27	0.28	0.56	0.64	3.47
35.4562.....	57.2245	F3	14.87	14.36	0.11	99	99	3.63
34.7824.....	57.2347	F9	15.10	14.47	0.30	0.56	1.37	4.55
34.9448.....	57.1925	F9?	15.12	14.51	0.45	0.90	1.48	5.65

Notes.—Faint MIPS excess sources that are consistent with membership in h and χ Persei. Spectral types for seven sources are derived from Hectospec data while the rest were inferred from J-band photometry. Values of 99 denote sources without 5 σ detections in a given band. Magnitudes given are the observed, not dereddened, values.

The 13 sources without known spectral types are either unobserved (12) or had a signal-to-noise ratio too low to derive spectral types (1; this source is well off the isochrone).

Many of the fainter 24 μm sources have high-quality IRAC photometry. Of the 17 MIPS excess sources fainter than $J = 13.5$ on the isochrone, 14 (12, 11) also have IRAC measurements at [4.5] ([5.8], [8]). We summarize the observed properties of the faint MIPS excess sources in Table 3. In the following two sections, we focus on these sources, comparing the MIPS photometry to IRAC/2MASS photometry from C07a and modeling the sources' emission from 2.2 to 24 μm.

3.3. *Nature of the Disk Population in Faint Pre–Main-Sequence Stars*

3.3.1. *Mid-IR Colors and the Wavelength-dependent Frequency of Disks*

To constrain the nature of the 17 faint MIPS excess sources that are (photometrically) consistent with cluster membership, we compare the $K_s/K_s - [24]$ CMD with CMDs using three IRAC colors, $K_s - [4.5]$, $K_s - [5.8]$, and $K_s - [8]$ in Figure 9 (*diamonds*). For reference, we also show the colors for bright MIPS sources without 24 μm excess (*squares*). Following C07a, we identify sources with $K_s - [\mathrm{IRAC}]$ colors ≥ 0.4 as IR excess sources; sources with $K_s - [24] \geq 0.65$ are 24 μm excess sources. A vertical line in Figure 9 shows the division between excess and non excess sources.

The frequency of IR excess varies with wavelength. Only 1/14 faint 24 μm excess sources also have excess at [4.5]. The fraction of sources with [5.8] excess is 3/12. The 8 μm excess population has a larger fraction of excess sources, 5/11. While some of the "photospheric' sources, $K_s - [4.5,\ 5.8,\ 8] \leq 0.4$, may have weak excesses, many sources have $K_s - [\mathrm{IRAC}] \leq 0.2$ (observed) and $\lesssim 0.1$ (dereddened). These sources are unlikely to have any dust emission at [4.5], [5.8], or [8]. While the small sample of 24 μm excess sources precludes a strong statistical significance for any trend of IR excess emission, the wavelength-dependent frequency of excess emission is consistent with results from larger surveys (e.g., C07a; Su et al. 2006).

3.3.2. *Temperature and Location of Circumstellar Dust*

Analyzing the strength of IR excess emission at multiple bands places constraints on the temperature and location of the dust. Just over half of the faint 24 μm excess sources have no excess emission in the IRAC bands, so these sources lack circumstellar material with temperatures $\gtrsim 400$ K. Because a blackbody that peaks at 24 μm has $T \sim 120$–125 K, the dust temperature in most of the faint 24 μm excess sources is probably $\lesssim 100$–200 K.

We can put more quantitative constraints on the dust temperature with a flux ratio diagram. Flux ratio diagrams have been an important tool in analyzing accretion disks in unresolved cataclysmic variable systems (e.g., Berriman et al. 1985; Mauche et al. 1997). In this method, the ratio of fluxes (in this case, λF_λ) at different wavelengths such as $\lambda_{4.5}F_{4.5}/\lambda_8 F_8$ and $\lambda_{24}F_{24}/\lambda_8 F_8$ is computed. The ratios for blackbody emission follow a curve in flux ratio space. Because disk-bearing sources should be, to first order, the sum of two blackbodies (a hot stellar component and a cooler circumstellar component), their positions in flux ratio space should lie on a line between the circumstellar dust temperature and the stellar temperature.

Figure 10 shows the flux ratio diagram for our sample, and Table 4 lists the derived disk temperatures (labeled as T_D FR). We restrict our sample to 10 sources with 5 σ detections from 4.5 through 24 μm.[8] Five of these sources have [8] excess; one has [4.5] excess. For 13–14 Myr old sources, the range of spectral types with $J = 14$–15.5 is $\sim$A0–G8 (Siess et al. 2000). The flux ratios for blackbody emission from 10 to 10,000 K follow the solid line with the temperatures characteristic of disks ($\sim$10–1000 K) on the vertical part of the line and those for stellar photospheres on the horizontal part. Loci showing the locations for a stellar photosphere+disk of a given temperature are shown ranging from $T_{\mathrm{disk}} = 300$ to 100 K assuming a stellar temperature of $T_{e,\star} \sim 7250$ K (about F0 spectral type). The sources without (with) IRAC excess emission, $K_s - [\mathrm{IRAC}] \lesssim 0.4$, are shown as

[8] The first source in Table 3, with $J = 13.84$, has a [8] flux that has a negative $K_s - [8]$ color and thus is unphysically faint. An unphysically large ratio of the [4.5] to [8] flux cannot be interpreted with a flux ratio diagram.

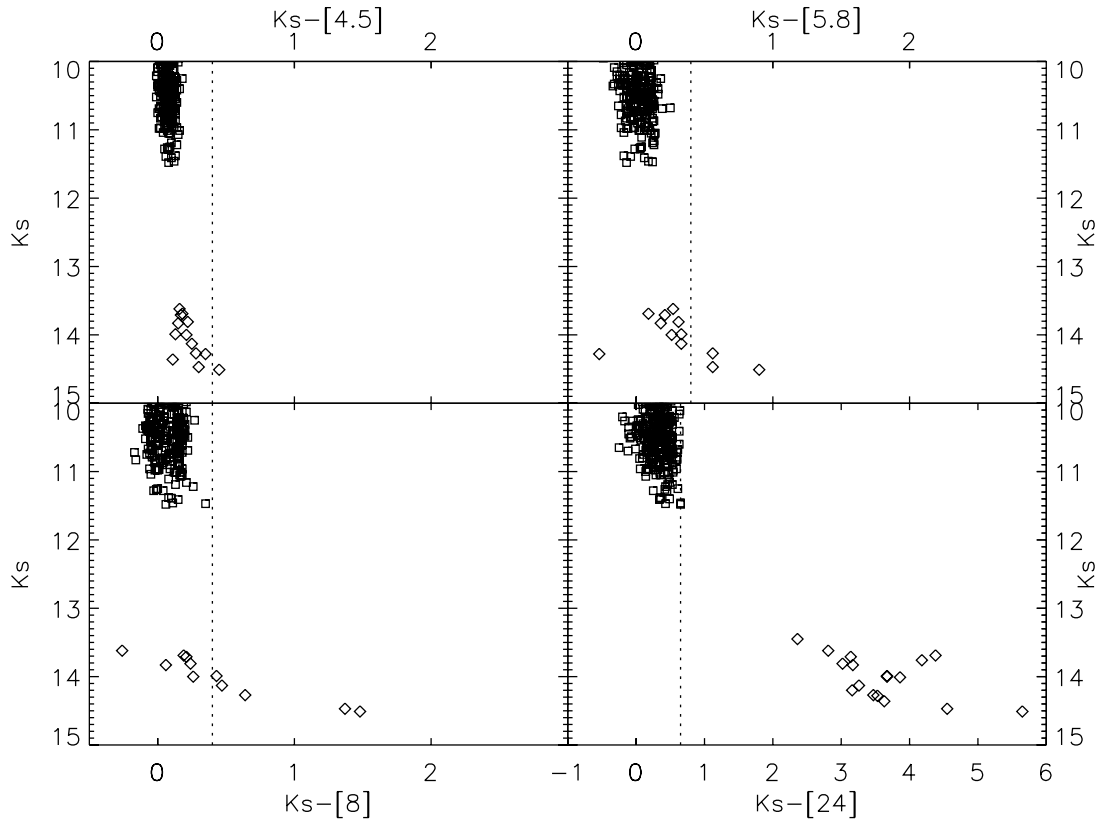

FIG. 9.—K_s vs. $K_s - [4.5]$, $K_s - [5.8]$, $K_s - [8]$, and $K_s - [24]$ color-magnitude diagrams for bright, photospheric sources and 24 μm excess sources. Of the 24 μm excess sources, 1/14 have excess at [4.5], 3/12 have excess at [5.8], and 5/11 have excess at [8].

diamonds (*thick diamonds*). The further away from the origin point of the loci a given source is, the more the disk contributes to the total flux. The derived dust temperatures are only weakly sensitive to $T_{e,\star}$ as flux ratios for 5250–10,000 K (∼G9–B8) blackbodies occupy roughly the same place at $\lambda_{4.5}F_{4.5}/\lambda_8F_8$ (∼5 ± 0.15) and $\lambda_{24}F_{24}/\lambda_8F_8$ (∼0). The line for the ice sublimation temperature is shown in bold. The source (diamond at ∼2, 0.5) with a disk component of ≈300 K has a strong [8] excess and was previously identified as having ∼300–350 K dust (source 5 in C07b) using a single blackbody χ^2 fit to the disk SED. Four other sources, also with 8 μm emission, have dust temperatures between 230 and 250 K. All the sources with 8 μm excess then have dust temperatures ≥230 K. While these sources may have cooler dust components, some of the dust emission must come from warmer disk regions closer to their parent stars.

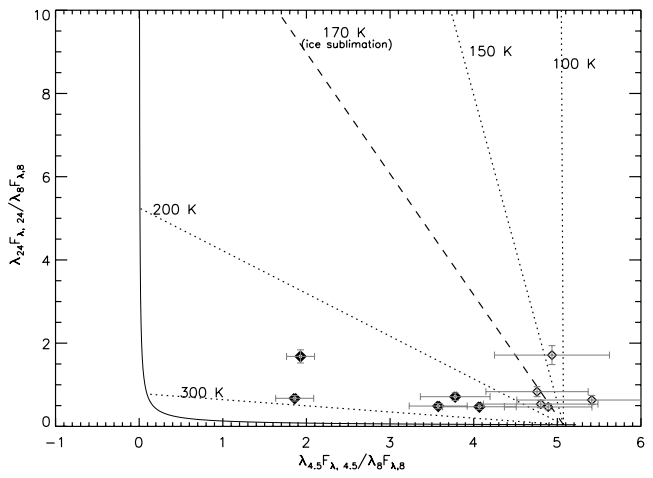

FIG. 10.—Flux ratio diagram for sources with 5 σ detections at 4.5 through 24 μm with errors in the flux ratios overplotted. The flux ratios for single temperature blackbodies are shown as a solid line. Dotted lines show loci of dust temperatures assuming a stellar blackbody temperature of 7250 K. Sources with 8 μm excess are shown in bold. The five sources with 8 μm excess typically have warmer dust temperatures ($T \sim 200$–300 K) indicative of terrestrial zone emission. The sources without 8 μm excess have colder dust temperatures. Two sources probably have some dust at temperatures comparable to the water ice sublimation point (170 K). Two sources probably have dust grains that are colder and icy (∼100–150 K). Typical errors for sources with only MIPS excess are ∼50 K, while errors for sources with IRAC and MIPS excess were smaller (∼20 K).

The dust temperatures of sources without 8 μm excess, characteristic of a slight majority in our sample, are significantly lower. Three sources have slightly cooler temperatures of ∼170–185 K, comparable to the water ice sublimation temperature (Hayashi 1981). The remaining sources have much cooler dust temperatures (∼100–150 K). This diagram demonstrates that many sources must have cold dust with temperatures of $T_{\rm dust} \lesssim 200$ K.

For sources with photospheric IRAC emission, using a single-temperature blackbody—calculated by matching the 24 μm excess while not producing significant excess in the IRAC bands—should match the observed disk emission well. However, many sources also have IRAC excess, and modeling the disk emission as coming from two sources (e.g., warm *and* cold dust) may yield a significantly better fit (e.g., Augereau et al. 1999). As an alternate way to constrain the disk temperature(s) and estimate the disk luminosity and location of the dust, we now consider blackbody fits to the dereddened SEDs. For sources with IRAC excess we add sources of hot and cold dust emission with temperatures of 50–250 and 250–700 K, respectively, to the stellar photosphere. Sources without IRAC excess are modeled by a stellar photosphere + single-temperature disk. For the stellar blackbody, we use the conversion from spectral type to effective temperature from Kenyon

TABLE 4
INFERRED PROPERTIES OF FAINT MIPS EXCESS SOURCES IN h AND χ PERSEI CONSISTENT WITH MEMBERSHIP

α	δ	SPECTRAL TYPE	T_d FR	T_d BB	χ^2	$L_\star$ ($L_\odot$)	$L_d/L_\star$	R_d (AU)	DISK TYPE
35.4339	57.0355	A2?	185	185	1.7	18.1	7×10^{-4}	9.75	CDD
35.3783	57.2056	A2?	170	175	5.7	18.1	5.5×10^{-4}	10.9	CDD
35.1178	57.2625	A3?	100	90	2.0	15.7	1.9×10^{-3}	38.4	CDD
34.7041	56.9259	A4?	130	120	6.0	12.8	3.5×10^{-3}	19.5	CDD
34.6889	57.2731	A6	230	85,375	7.6	12	3.1×10^{-3}	1.8,37.0	WDD
34.8108	57.4067	F2?	170	165	3.1	6.7	2.3×10^{-3}	7.5	CDD
35.3215	57.2030	F9	240	220,305	3.2	6.1	1.9×10^{-3}	2.1,4	WDD
35.1171	57.2662	F9?	250	175,400	5.8	6.1	2.3×10^{-3}	1.2,6.3	WDD
34.7824	57.2347	F9	300	240,330	0.5	6.1	6.3×10^{-3}	1.8,3.4	WDD
34.9448	57.1925	F9?	230	110,435	5.1	6.1	1.5×10^{-2}	1.0,16.0	TWH

NOTES.— Inferred properties of faint MIPS excess sources with photometry at multiple bands. The SEDs of 10 sources were constrained well enough to derive disk temperatures from flux ratio diagrams (T_D FR) and from fitting the source SEDs to star + one (two) blackbody disk populations (T_D BB) for sources without (with) IRAC excess. The location of the dust (R_D) is derived from simple blackbody equilibrium. Relative disk luminosities ($L_D/L_\star$) were derived assuming a stellar luminosity from stars of a given spectral type at the age of h and χ Per from Siess et al. (2000). For the evolutionary states, WDD = warm debris disk (which have colder components), CDD = cold debris disk, and TWH = Hya-like source that may be optically thick at long wavelengths.

& Hartmann (1995). If the star has no spectral type, we use the dereddened J band flux as a proxy for spectral type as in C07a, assuming $A_J \sim 0.45$ and using the Kenyon & Hartmann (1995) conversion table, and add a question mark after the spectral type in Tables 3 and 4. We use the stellar luminosity, $L_\star$, for 13–14 Myr old stars of a given spectral type from Siess et al. (2000). A χ^2 fit to the 3.6–24 μm fluxes is performed to find the best-fit one or two dust blackbody + stellar blackbody model following Augereau et al. (1999). Following Habing et al. (2001), we derive the disk luminosity from blackbody fits. The integrated fluxes for each dust population of a given temperature are added and then divided by the stellar flux to obtain the fractional disk luminosity, $L_D/L_\star$. Finally, we estimate the location of the dust populations from simple radiative equilibrium:

$$R(\mathrm{AU}) \approx (T_{\mathrm{disk}}/280)^{-2}(L_\star/L_\odot)^{0.5}. \quad (1)$$

The sources without IRAC excess have nearly identical disk temperatures to those derived from the flux ratio diagram (Table 3), ranging from ~90 to 185 K, and are similar to equilibrium temperatures just beyond the terrestrial zone into the gas giant regions of the solar system. These sources have χ^2 values slightly less than or comparable to the number of observations (~1–6). The fractional disk luminosities range from $\sim 5.5 \times 10^{-4}$ to 3.5×10^{-3}, which is similar to dust luminosities for young stars surrounded by optically thin debris disks (e.g., Meyer et al. 2007). Dust in these systems is probably confined to disk regions of ~8–40 AU.

Sources with both IRAC and MIPS excess emission have disk temperatures substantially different from those inferred from the flux ratio diagram and show evidence of terrestrial zone dust emission and colder dust.

The two dust population fits for the IRAC+MIPS excess sources show evidence for a wide range of dust temperatures with warm terrestrial dust emission and cold dust emission similar to that from sources without IRAC excess. For instance, the SED of the A6 star with IRAC and MIPS excess is best fit ($\chi^2 \sim 7.6$) by a hot dust component of 375 K coming from 1.8 AU and a cold component of 85 K at ~37 AU. The faint F9 star, identified previously as "source 5," is extremely well fit ($\chi^2 \sim 0.5$) by dust populations of 240 and 330 K at 1.8 and 3.4 AU, respectively. Because these sources have both warm and cold dust, it is not surprising that their fractional disk luminosities are typically higher. The fractional luminosity of source 5 ($\sim 6 \times 10^{-3}$) is comparable to the most massive debris disks (e.g., HR 4796A), and in general the luminosity of the disk population is consistent with values for massive debris disks. The most luminous disk source ($L_D/L_\star \sim 1.5 \times 10^{-2}$) is the lone exception and has a luminosity halfway in between values expected for luminous debris disks (~several $\times 10^{-3}$) and long-lived T Tauri disks with inner holes (e.g., TW Hya; Low et al. 2005). We analyze this system further in § 3.3.3.

In summary, the faint MIPS excess sources have dust with a range of temperatures and luminosities. Sources without IRAC excess are well fit by single-temperature blackbodies and have cold dust components with temperatures ~90–185 K. Sources with IRAC excess are better fit by two dust components, a hotter, terrestrial zone component and a cooler component. The disks in h and χ Persei then show evidence of having inner regions of varying sizes cleared of dust. All but one source has a fractional disk luminosity $\lesssim 10^{-2}$, consistent with optically thin debris disks. In the next section, we investigate the evolutionary state of the faint MIPS excess population further by comparing their properties to other predicted properties for massive debris disks and T Tauri disks.

3.3.3. *Evolutionary State of the MIPS Disk Candidates: A Population of Luminous* ~13–14 Myr *Old Debris Disks*

We now consider the evolutionary state of the dust in the 24 μm excess sources. Although the relative luminosities ($L_d/L_\star \sim 10^{-3}$) and lack of accretion signatures suggest these h and χ Per sources are debris disks, some T Tauri stars (e.g., "transition" T Tauri stars; Kenyon & Hartmann 1995) may also have inner regions cleared of gas and dust. Thus, it is important to compare their disk properties to models of debris disks and T Tauri disks.

We first examine the nature of the h and χ Per disk population as a whole. Because our smallest disk luminosities, $\sim 5 \times 10^{-4}$, are larger than more than half of known $\gtrsim$10 Myr old disks (e.g., Meyer et al. 2007), our MIPS sample probably misses lower luminosity sources with $L_d/L_\star \lesssim 10^{-4}$. Similarly, our lack of 70 μm detections limits our ability to detect and to evaluate disk emission from cooler dust—such as is observed in β Pic and HR 4796A—with SEDs that peak at 40–100 μm. For example, the nearby, luminous disk around 49 Cet (spectral type A1 V, 8 Myr old; Wahhaj et al. 2007) has a 24 μm excess of ~2.5 mag. We detect

only one faint ($J \geq 13$) MIPS excess sources with $K_s - [24] \leq 2.5$. Therefore, it is possible that there are additional very luminous young disks in h and χ Per just below our detection limit.

These limits and the rich nature of the Double Cluster allow us to estimate the prevalence of massive, luminous disks. The total number of A0 to early F stars (F2) in h and χ Per is $\approx$1000 (T. Currie et al. 2007, in preparation; cf. C07a). Assuming that the disk fraction is $\sim$20%,[9] we detect 17/200, or $\approx$10% of all disks with strong emission at 24 μm. Thus, this population is extreme and yields a better understanding of the evolutionary state of the most luminous disks in a populous star cluster.

To constrain the evolutionary state of the disks, we compare the near- to mid-infrared disk colors to those expected for two disk models: a flat, optically thick disk around a classical T Tauri star ($T_{\rm disk} \sim r^{-0.75}$; Kenyon & Hartmann 1987) and an optically thin disk model from Kenyon & Bromley (2004a) for debris emission produced by planet formation. Because only one of our sources has [4.5] excess emission and less than half have [8] excess emission, we match the data to models of planet formation not in the terrestrial zone (Kenyon & Bromley 2004a) but at 30–150 AU from a 2.0 $M_\odot$ primary star (Kenyon & Bromley 2004b). For a $\sim$2.0 $M_\odot$, 20 $L_\odot$ star, the temperature range from 30 to 150 AU is comparable to the outer gas/ice giant region in our solar system ($\sim$6.7–34 AU). We adopt a $\Sigma \propto r^{-1.5}$ profile for the initial column density of planetesimals and an initial disk mass of 3 times a scaled minimum mass solar nebula (Hayashi 1981): $3 \times 0.01 M_\star/M_\odot$ (where $M_\star = 2\,M_\odot$). Emission from planetesimal collisions is tracked for $\sim 10^8$ yr. Model predictions are reddened to values for h and χ Persei (reddening laws in the IRAC/MIPS bands are described in C07b).

Figure 11 shows the $K_s - [4.5,\ 5.8]/K_s - [24]$ color-color diagrams for bright photospheric sources and the faint 24 μm excess sources. The debris disk locus is overplotted as a thin black line. Debris from planet formation produces a peak excess emission at $K_s - [24] \sim 3.6$ at $\sim 10^7$ yr; the $K_s - [4.5]$ and $K_s - [8]$ colors peak at $\sim$0.4 at earlier times ($\sim 10^6$ yr). The debris disk locus tracks the colors for most of the sources in $K_s - [4.5]/K_s - [24]$ space very well (Fig. 11*a*). While the locus underpredicts the [8] excess for about half of the sources (Fig. 11*b*), warmer regions of a debris disk not modeled here may produce this excess (e.g., Kenyon & Bromley 2004a). C07b showed that planet formation in the terrestrial zone can produce strong [8] emission characteristic of some h and χ Per sources at $\sim$10–15 Myr. Indeed, the source with $K_s - [8] \sim 1.3$, $K_s - [24] \sim 4.4$ is source 5 from C07b, which was one of eight modeled as having terrestrial zone debris disk emission. The warm dust temperature ($\sim$300 K) derived for this source in § 4.2 is consistent with terrestrial zone emission.

Disk models corresponding to earlier evolutionary states fare worse in matching the observed mid-IR colors. The optically thick flat disk model (*triangle in both plots*) predicts $K_s - [5.8]$ ([8]) $\sim$ 1.5 (2.9) and $K_s - [24] \sim 6$, consistently 1–2 mag redder than the data. To match the observed [24] excess, any optically thick disk with an inner hole (cf. C07b) must be cleared of dust out to the distances probed by the MIPS bands: $\sim$25 AU for a 20 $L_\odot$ primary star. While inner hole models may be constructed to fit the SEDs of sources with only 24 μm excess, these models predict nearly zero IRAC color even though about half of the sample has excess at [8]. Lack of gas accretion signatures, low fractional disk luminosities, and SED modeling then suggest that at least many faint h and χ Per sources with 24 μm excess are stars surrounded by optically thin debris disks. More sensitive spectroscopic observations are needed to verify the lack of gas in these systems.

[9] Disk fractions quoted by Chen et al. (2005b) range from 9% to 46%.

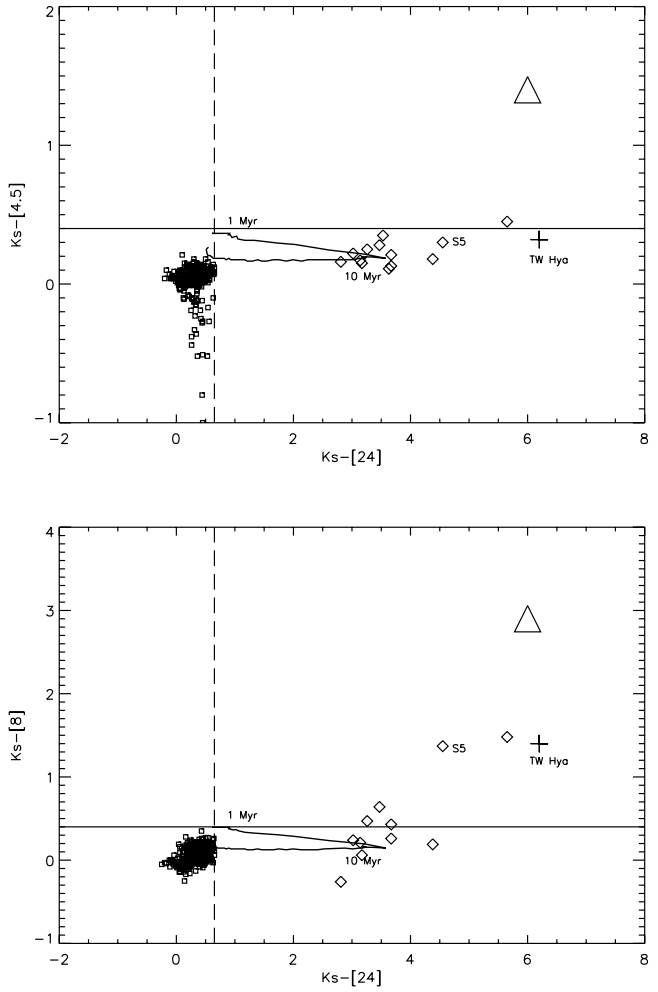

FIG. 11.—Color-color diagrams $K_s - [3.6]/K_s - [24]$ (*top*) and $K_s - [8]/K_s - [24]$ (*bottom*). Sources below the horizontal line have photospheric [4.5] emission; those to the left of the vertical line have photospheric [24] emission. The source with $K_s - [8] \sim 1.3$ and $K_s - [24] \sim 4.5$ is source 5 in C07b and is labeled "S5." One source appears to have mid-IR colors strongly resembling TW Hya (*shown as a large cross*; reddened to h and χ Per). All sources have colors inconsistent with an optically thick primordial disk (*large triangle*). The debris disk locus is overplotted as a dark solid line with reddened $K_s - [24]$ colors at 1 Myr ($\sim$0.9) and 10 Myr ($\sim$3.2) labeled. Debris from planet formation at 30–150 AU accurately reproduces the $K_s - [4.5]/K_s - [24]$ diagram colors and is able to reproduce the $K_s - [8]$ colors for sources with weaker [8] excess.

Despite the general success of the debris disk models, at least one h and χ Per source may harbor a disk at an earlier evolutionary state. This source has a $K_s - [24]$ color of $\sim$6, which is $\sim$1 mag redder than HR 4796A, the strongest 24 μm excess source in R05. This color is close to the optically thick disk predictions, is extremely difficult to produce with a debris disk model, and is more similar to the level of excesses in older T Tauri stars like HD 152404 and TW Hya (Chen et al. 2005b; Low et al. 2005).

To explore this possibility, we overplot the $K_s - [4.5]$, $K_s - [8]$, and $K_s - [24]$ colors of TW Hya from Hartmann et al. (2005) and Low et al. (2005) in Figure 11 (reddened to h and χ Per; *large cross*). The mid-IR colors of our brightest source are similar to the colors of TW Hya. While TW Hya's disk has an optically thin inner region where the early stages of planet formation may be commencing (Eisner et al. 2006), the disk is probably optically thick at 24 μm (Low et al. 2005). TW Hya also has strong Hα emission which indicates accretion. On the other hand, the fractional

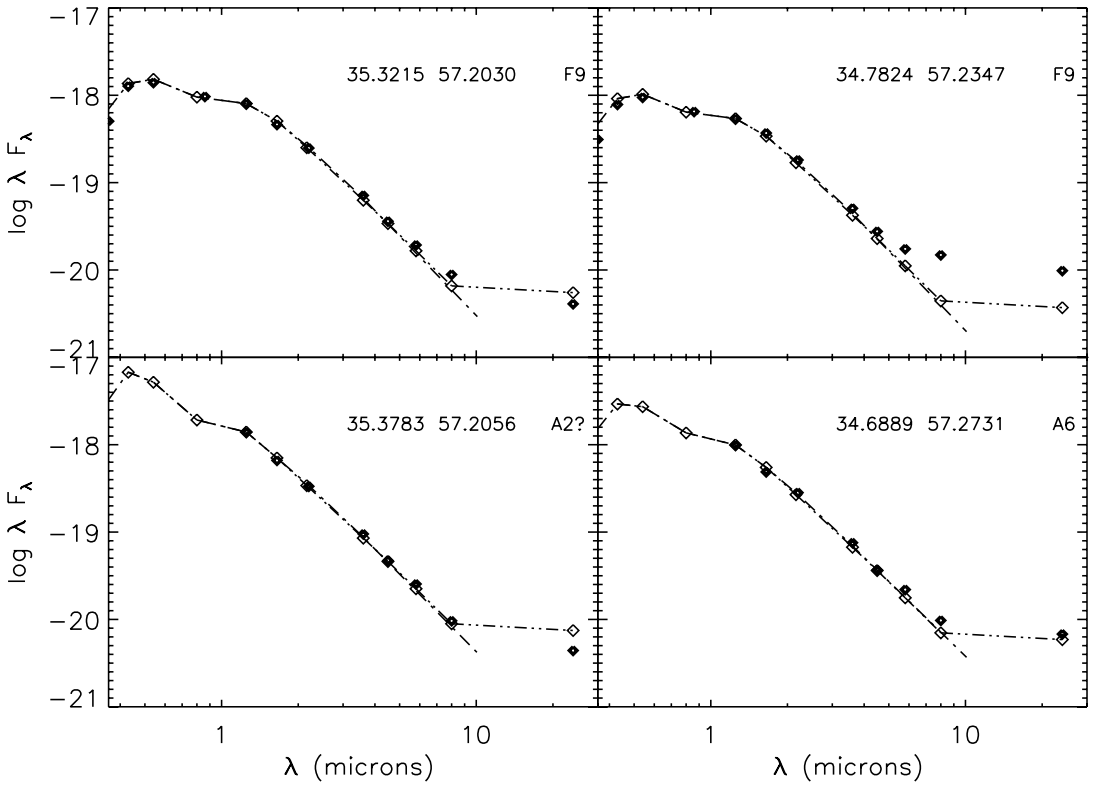

FIG. 12.—SEDs for selected MIPS-excess sources. The J2000 coordinates of the sources (in degrees) are 35.3215, 57.2030 (1); 34.7824, 57.2347 (2); 34.6889, 57.2731 (3); and 35.3783, 57.2056 (4). The spectral types of the sources are (*clockwise from the top*) F9, F9, A6, and A2. The photospheric model (*dash-dot line*) and cold debris disk model (*dash-double dotted line*) from Kenyon & Bromley (2004b) are overplotted. The top right F9 source was modeled as having terrestrial zone emission, although the disk may extend to more distant, cooler regions. Two sources (F9 and A6, *top left*) exhibit weak 8 μm emission, whereas the A2 source, typical of the majority of faint MIPS-excess sources, has no excess emission at 8 μm.

disk luminosity in h and χ Per sources is much lower than that of TW Hya ($\sim$0.27; Low et al. 2005) and between the values for debris disks and transition disks. Thus, some lines of evidence suggest that this extreme h and χ Per source is at an evolutionary state earlier than the debris disk phase, while others are more ambiguous. Obtaining optical spectra of this source, to search for accretion signatures, may allow us to make a better comparison between it and older T Tauri stars like TW Hya.

The spectral energy distributions (SEDs) of the faint MIPS excess sources show evidence for a range of dust temperature distributions, which may be connected to a range of evolutionary states (Fig. 12). We select four sources, three with spectra and one without, that are representative of the range of mid-IR colors from our sample. The first three sources of Figure 12, dereddened to $A_V = 1.62$ [$E(B-V) = 0.52$], have been spectroscopically confirmed as F9 (source 1), F9 (source 2), and A6 (source 3) stars, respectively; the second source was mentioned in the previous paragraph [with $K_s - [24] \sim 4.4$. The SEDs for the bottom left source was also dereddened to $A_V = 1.62$, and a spectral type of A2 was chosen based on the conversion from absolute magnitude to spectral type for 14 Myr old sources (from Siess et al. 2000; Kenyon & Hartmann 1995 color conversions). The source with photospheric emission at $\lambda < 24$ μm (source 4) has IRAC colors representative of just over half of the faint MIPS-excess sources in Figure 11. The debris disk model accurately predicts the SEDs of the source with photospheric 8 μm emission and two sources with weak 8 μm excess emission. The remaining source is not fit well by the disk model and shows clear evidence for a large warm dust population (see C07b). The evolutionary states for the sources shown in Figure 12 and the nine sources with complete IRAC and MIPS photometry are listed Table 2.

Thus, we conclude that emission from at least half of the 24 μm excess sources around pre–main-sequence stars in h and χ Per is best explained by debris from planet formation at locations comparable to the gas/ice giant regions in the solar nebula. Some of the other pre–main-sequence stars with 24 μm excess may also have ongoing planet formation in the inner, terrestrial zone regions as indicated by their 8 μm excesses. One of our sources may be a T Tauri star at a slightly earlier evolutionary state than the debris disk sources in our sample.

If most of the disk population is then interpreted as an early debris disk population (not a Class II/III transition T Tauri disk population), the wavelength-dependent frequency of IRAC/MIPS disk excess identified in § 3.3.1 implies a location-dependent evolution of debris disks, specifically a clearing of warm dust from inner disk regions. This behavior is consistent with standard models of planet formation (Kenyon & Bromley (2004a), which predict that dust emission from the planet formation process disappears at shorter wavelengths (e.g., IRAC bands) faster than at longer wavelengths (e.g., MIPS bands). This result is expected if planet formation runs to completion in the innermost regions of protoplanetary disks before planets are formed in the outer disk.

4. EVIDENCE FOR A RISE AND FALL OF DEBRIS DISK EMISSION

To place our results in context, we now compare the excesses observed in h and χ Per sources with measurements of other stars with roughly similar masses. We follow R05 and consider the magnitude of the 24 μm excess, $[24]_{obs} - [24]_{\star}$, as a function of time. Using a sample of early (A) type stars with ages $\gtrsim$5 Myr, R05 showed that stars have a wide range of excesses at all ages and that sources with the largest excesses define an envelope

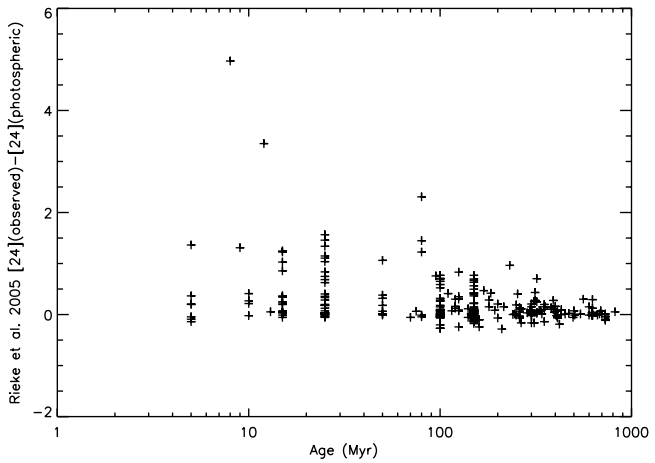

FIG. 13.—*Top:* Color-excess of sources from the R05 sample assuming that the photospheric $K_s - [24]$ color is ~0. The strongest excess sources in this sample are HR 4796A (8 Myr) and β Pictoris (12 Myr). There is a clear trend of decreasing color excess vs. age beyond ~20 Myr.

that decays slowly with time (Fig. 13). Although this envelope is consistent with a power-law decay, $[24]_{\rm obs} - [24]_\star \propto t^{-1}$, the R05 sample has relatively few stars with ages ~5–20 Myr where debris disk models predict large excesses. The sources with the largest excesses, HR 4796A and β Pic, fall within this age range at 8 and 12 Myr,[10] respectively.

Together with our results for h and χ Per, several recent surveys in young clusters and associations identify debris disks with ages of ~5–20 Myr (Chen et al. 2005b; Hernandez et al. 2006; Sicilia-Aguilar et al. 2006). As in R05, these surveys show a large range of 24 μm excesses at each age. In the well-sampled Sco-Cen Association, for example, Chen et al. (2005b) identify many stars with photospheric emission (no excess) at 24 μm and several stars with excesses considerably larger than the typical excess observed in the R05 sample. Although our h and χ Per data do not provide any measure of the number of stars with photospheric emission at 24 μm, the survey yields a good sample of stars with excesses much larger than the typical R05 source.

We now combine our results with those from R05 and from more recent surveys of debris disks in young clusters. Specifically, we add data from Tr 37 (4 Myr) and NGC 7160 (11.8 Myr) (in Cepheus; Sicilia-Aguilar et al. 2006), Orion OB1a (10 Myr), and Orion OB1b (5 Myr; both from Hernandez et al. 2006), and Sco-Cen (~5, 16, and 17 Myr for Upper Sco, Lower Centaurus Crux, and Upper Centaurus Lupus, respectively; Chen et al. 2005b). For h and χ Per and Cepheus sources, we include only the IR-excess sources. The sensitivity of the Sco-Cen observations allows more precise determinations of the photospheric flux levels farther down the initial mass function of the cluster, so we include data for all sources earlier than G0 with or without excess in this cluster. For sources with no published estimate of the photospheric flux, we assume that $K_s - [24]_\star \sim 0$ (dereddened), which is valid for our sample of A and F stars.

4.1. *Observed Mid-IR Emission versus Age*

When data from h and χ Persei and other young clusters are added to R05, the evolution of 24 μm excess with age shows an important new trend. *From* ~5–10 Myr, *there is a clear rise in the magnitude of excess followed by a peak at* ~10–15 Myr, *and a slow* t^{-1} *decay after* ~15–20 Myr (Fig. 14). All sources with very large (≳3 mag) excesses have ages between 8 and 16 Myr. The 24 μm excess emission peaks at ~12–16 Myr as indicated by strong excess sources in h and χ Persei (*diamonds*), NGC 7160 (*squares*), and Sco-Cen (*asterisks*). Data from 5 Myr old Orion OB1b and Upper Sco to 10 Myr old Orion OB1a to 12–17 Myr old NGC 7160, h and χ Per, and the two older Sco-Cen subgroups shows a sequential rise in the median 24 μm excess.[11] A peak in the 24 μm excess emission at ~10 Myr is also visible in a plot from Hernandez et al. (2006), albeit at a lower statistical significance. The addition of several ≲20 Myr old clusters more strongly constrains the time when debris emission peaks and maps out its evolution from 5–20 Myr in more detail.

Removing possible TW Hya–like sources from this diagram does not modify the trends. The "TW Hya–like" source in h and χ Per ([24] excess ~5.5) and the strongest excess source in Sco-Cen ([24] excess ~5.75) have the largest 24 μm excesses and may be at an evolutionary state prior to the debris disk phase. However, many sources in the 10–15 Myr age range have ~2–3.5 mag excesses, including HR 4796A and many h and χ Per sources, which have disk luminosities and mid-IR colors inconsistent with an optically thick disk. The second most luminous source in Sco-Cen, HD 113766A (F3 spectral type) with a 24 μm excess of ~4.7 mag, has a fractional disk luminosity characteristic of a massive debris disk (Chen et al. 2005b). Sources with $[24]_{\rm obs} - [24]_\star \geq 2$–3 are more common at ~10–15 Myr than at much younger (~5 Myr) or older (≳20 Myr) ages.

4.2. *Statistical Verification of a Peak in* 24 μm *Emission at* 10–15 Myr

The peak at 10–15 Myr is statistically robust. To test it, we adopted the underlying approach that Wyatt et al. (2007b) demonstrate gives a good first-order description of debris disk behavior: debris disks all evolve in a similar fashion, with the variations among them arising primarily from differences in initial mass. This result has two important implications for us: (1) it validates deducing evolution with time from the upper envelope of the infrared excesses, since similar high-mass disks of different ages define this envelope; and (2) it allows us to estimate the distribution of excesses at any time by scaling the excesses at another time according to t^{-1} (by one over the ratio of the source ages), the general time dependence of disk decay (R05). We use the second of these results to predict the distribution of excesses at 5 Myr from measurements of the distribution at 10–30 Myr, where enough systems have been measured to define the distribution well. We use three samples (Sco-Cen, Orion Ob1, and R05), each of which includes the complete range of $[24]_{\rm obs} - [24]_*$ down to zero, i.e., photospheric colors. If the scaled colors for sources predict much larger excesses than the 5 Myr old Orion Ob1b excesses, then we can conclude that the mid-IR colors of our samples from 5 to 15 Myr do not follow a t^{-1} decline.

Figure 15 shows the scaled Sco-Cen and Rieke et al. excesses compared to the observed 5 Myr excesses in Orion Ob1b normalized to the total number of sources in each sample. Many scaled excess sources (~20% of the total population) are ≳1–3 mags redder than any in Orion Ob1b. The Kolmogorov-Smirnov (K-S) test shows that the scaled Sco-Cen (Rieke et al.) sources have a

[10] While β Pictoris was given an age of 20 Myr in R05, derived from Barrado y Navasceus et al. (1999), recent work suggests a slightly younger age of ~12 Myr (e.g., Zuckerman et al. 2001; Ortega et al. 2002).

[11] The debris disk candidates in Tr 37 have larger excesses than those in Orion OB1a. However, the strong excess may be explained by differences in stellar properties: two-thirds of the debris disk systems in Tr 37 are B3/B5 and B7 stars, which are far more massive than 10 Myr old A/F stars (~3.5–6 $M_\odot$ vs. 1.5–2.5 $M_\odot$; cf. Siess et al. 2000). If typical disk masses scale with the stellar mass, then these much more massive stars should have more massive, more strongly emitting disks. The disk mass-dependent amplitude of excess is discussed in § 4.3.

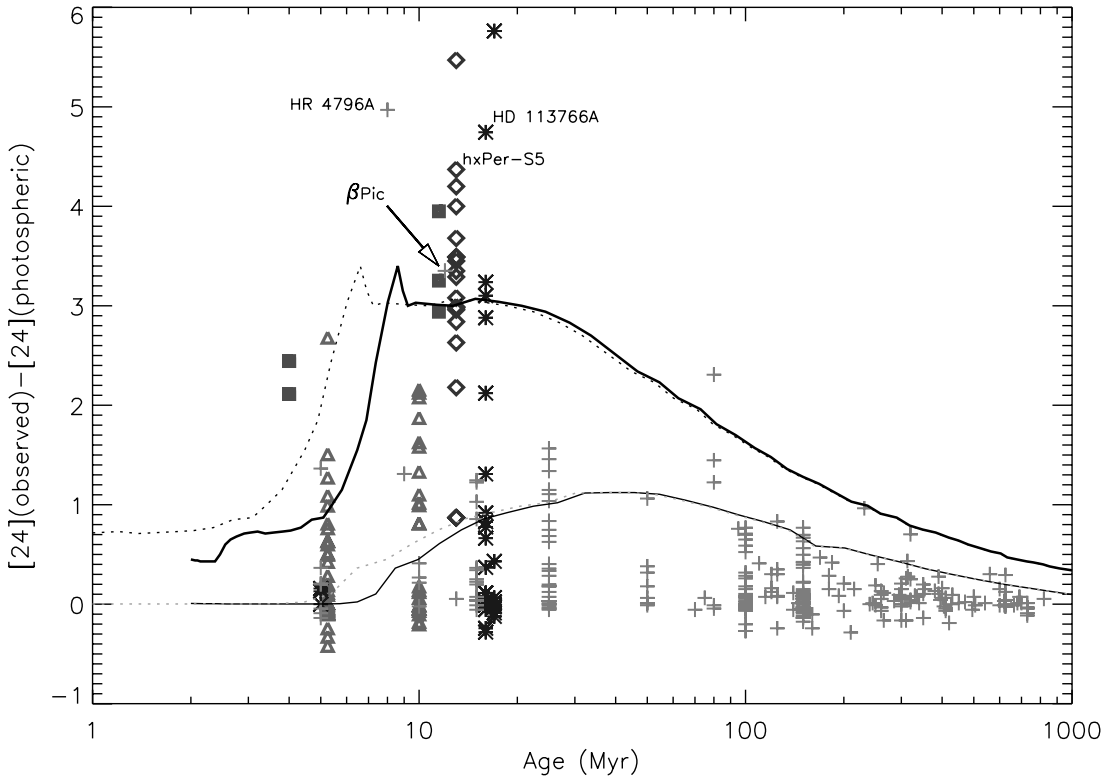

FIG. 14.—Color-excess of sources from R05, as well as ~13 Myr old h and χ Persei (*diamonds*); Sco-Cen subgroups at 5, 16, and 17 Myr old (*asterisks*; Chen et al. 2005b); 4 and 11.8 Myr old Cepheus subgroups Tr 37 and NGC 7160 (*squares*; Sicilia-Aguilar et al. 2006); and 5 and 10 Myr old Orion Ob1b and Ob1a (Hernandez et al. 2006). We include the B4 star in h and χ Per with MIPS excess. HR 4796A is again clearly visible while β Pic is obscured by the Cepheus data. Upper Sco data (5 Myr old) is also obscured by Orion Ob1b and has 24 μm excess ~0–0.3. Overplotted are debris disk evolution tracks from Kenyon & Bromley (2004b) for a 3 times and $\frac{1}{3}$ times the (scaled) MMSN disk, assuming that primordial disk grains grow to planetesimal sizes by 0 (*dotted line*) and 2 Myr (*solid line*). There is a clear trend of increasing color excess at 24 μm from ~5–10 Myr, a peak at ~10–15 Myr, and a steady decline afterward through 1 Gyr. The trend is clear even if the strongest excess sources in h and χ Per and Sco-Cen ($[24]_{obs} - [24]_{\star} \gtrsim 4$–5) were excluded due to their uncertain evolutionary states.

probability of 0.07 (0.06) of being drawn from the same population as Orion Ob1b with a ≳0.75 mag excess. If we instead compare the scaled sources to Orion Ob1b sources with a ≳0.5 mag excess, where Orion and the other two populations begin to overlap in Figure 15, the probability is even lower: 2.3×10^{-5} (3.5×10^{-8}) for the Sco-Cen (Rieke et al.) sample. Thus, the evolution of 24 μm emission from Orion Ob1b, Sco-Cen, and Rieke et al. sources is not consistent with a t^{-1} decay.

There are two main alternatives to the t^{-1} decay of IR excess with time for the youngest debris disks. The IR excess could be constant for ~20 Myr and then follow a t^{-1} decay law. The IR excess could also increase with time to some peak value and then follow a t^{-1} decay law. To test the constant emission possibility, we use the Wilcoxon rank sum test. The rank sum test allows us to evaluate whether or not the populations have the same mean value or have intrinsically larger/smaller excesses than another sample (Z parameter). The test also measures the probability that two samples are drawn from the same parent population by the Prob(RS) parameter (as in the K-S test).

Table 5 summarizes our results. Statistical tests show that the $[24]_{obs} - [24]_{\star}$ excesses cannot be constant with time and verify that emission rises from 5 to 10 Myr (Table 3). Sco-Cen has the largest mean excess ratio (~1.25) and has the widest range of colors with a $[24] - [24]_{\star}$ standard deviation of ~1.4 compared to ~0.6–0.8 for the Orion subgroups. The Wilcoxan rank sum test reveals that Sco-Cen has ≲5% probability of being drawn from the same population as Orion Ob1b and has a statistically significant larger peak ($Z \sim -1.65$). Orion Ob1a also has a significant larger peak than Orion Ob1b [$Z \sim -2.8$,

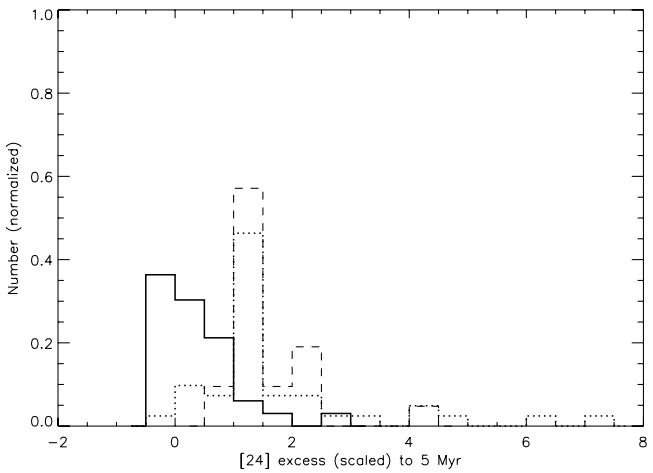

FIG. 15.—$[24] - [24]_{\star}$ excesses for Orion Ob1b (*solid line*) compared to the "scaled" 5 Myr Sco-Cen (*dotted line*) and Rieke et al. colors (*dashed line*), assuming that excess emission declines as t^{-1} for $t \gtrsim 5$ Myr. We normalize the total number of sources in each bin by the total number of sources in all bins. The excesses from many Sco-Cen and Rieke et al. sources are far redder than any Orion sources (≳4 mag). Thus, the evolution of 24 μm emission from disks is not consistent with a t^{-1} power law. Further statistical tests, described in § 4.2, verify that the emission rises from 5 to 10 Myr.

TABLE 5
Statistical Tests for Complete Samples of MIPS-detected Stars

Group	Age (Myr)	$[24] - \bar{[24]}_\star$ (All)	$[24] - \bar{[24]}_\star$ (Excess)	$\sigma([24]-[24]_\star)$	RS Z (Excess)	RS Prob (Excess)
Sco-Cen	16	0.67	2.10	1.41	−1.65 (−0.05)	0.05 (0.48)
Orion Ob1a	10r	0.72	1.46	0.83	−2.8 (0)	0.002 (1)
Orion Ob1b	5	0.36	0.91	0.63	0 (2.8)	1 (0.002)

Notes.—Statistics comparing the populations of Sco-Cen, Orion Ob1a, and Orion Ob1b. We calculate the mean ($[24] - [24]_\star$) color (for the entire sample and for "excess" sources), the standard deviation (σ) of each sample's colors, and the Wilcoxan rank sum probability and Z parameter. Here "excess" sources denote those with $[24] - [24]_\star \gtrsim 0.25$. The first (second) entry in the rank sum test statistics compares each population to Orion Ob1b (Orion Ob1a). A positive Z parameter means that the sample has a larger peak value than Orion Ob1b (first entry) and Orion Ob1a (second entry). A low rank sum probability means that the $[24] - [24]_\star$ colors of the populations are very different. These results show that Sco-Cen and Orion Ob1a have statistically significant larger 24 μm excesses than Orion Ob1b. Sco-Cen and Orion Ob1a have similar populations, although Sco-Cen has larger mean excesses and a larger dispersion in excesses.

Prob(RS) ~ 0.002], and Sco-Cen's peak is marginally larger than Orion Ob1a's ($Z \sim -0.05$).

These results lead us to conclude that *the evolution of mid-IR excess emission from planet formation in debris disks is best characterized as a rise in excess from* ~5–10 Myr, *a peak at* ~10–15 Myr, *and a fall in excess from* ~15–20 Myr *to* 1 Gyr. The rise to maximum excess from 5 to 10 Myr is steep: typical excesses increase from ~1 to ~3 mag by 11.8 Myr. The peak in excess amplitude is ~5–10 Myr broad because the excesses in NGC 7160, h and χ Per, and Sco-Cen are all comparable. By ~25 Myr the typical excesses decline with age as suggested by R05.

4.3. *Comparison with Models of Emission from Planet Formation*

To investigate how the "rise and fall" trend of debris emission may be connected with physical processes producing the emission, we overplot the debris disk evolution tracks (*dotted lines*) from § 3.3.3 and debris disk tracks for a low-mass disk ($\frac{1}{3} \times \mathrm{MMSN_{scaled}}$). The Kenyon & Bromley (2004b) calculations start at $t = 0$ with an ensemble of ~kilometer-sized planetesimals. To bracket the likely timescale for kilometer-sized planetesimals to form at 30–150 AU (e.g., Dominik & Dullemond 2005; Weidenschilling 1997), we include a second locus shifted by 2 Myr (*solid lines*). The range in debris disk masses is about a factor of 10, comparable to the range of disk masses inferred from submillimeter observations of young stars (Andrews & Williams 2005).

The debris disk models from § 3.3.3 show a steep increase in debris emission from 5–10 Myr, a plateau for the following ~20 Myr, and then a shallow decline in debris emission. The massive disk locus (*dotted line*) yields a peak in emission at ~7–8 Myr, or very close to the age of HR 4796A. The locus started at 2 Myr (*solid line*) peaks at ~9–10 Myr, close to the ages of h and χ Persei and NGC 7160, and yields substantial emission through 20 Myr before emission declines. The lower mass disk loci peak later at ~40 Myr with excesses comparable to the majority of those in R05. Caution should be taken to avoid overinterpreting these similarities: the exact time of the debris disk emission peak as well as the amplitude of the peak depend on input parameters such as planetesimal disruption energy.

Nevertheless, the massive debris disk model yields the same general trend in the maximum 24 μm excess amplitude with time; the low-mass disk model reproduces the 24 μm excesses of many ≳30 Myr old sources. The observed behavior of 24 μm excess with time is then at least qualitatively consistent with our understanding of the processes associated with planet formation.

5. DISCUSSION

5.1. *Summary of Results*

Our analysis of MIPS data for the 13–14 Myr old double cluster, h and χ Persei, shows two significant 24 μm excess populations. Bright Be stars with $J \lesssim 12$–13 have 1–2 mag excesses at 24 μm and follow a clear Be star locus in the $J - H/H - K_s$ color-color diagram. Optical spectra confirm the Be star status for just under half of the candidates from the color-color diagram. We also detect a B4 star with a clear 24 μm excess but without Hα emission or evidence for near-IR excess.

Fainter stars with $J \sim 14$–15 fall on the 14 Myr isochrone in a $J/J - H$ color-magnitude diagram. Optical spectra confirm that many of these stars have late A-type or F-type spectra, consistent with cluster membership. The IRAC and MIPS colors of these sources suggest that the frequency of excess at wavelengths which probe IR excess emission increases with increasing wavelength. The wavelength-dependent frequency of excess is consistent with the presence of inner holes devoid of dust.

Our analysis of the dust temperatures in the fainter excess sources suggest two groups. A smaller group of stars has emission from warmer dust with $T \sim 200$–300 K. A larger group has emission from colder dust, $T \lesssim 200$ K. In both groups, the dust luminosity is a small fraction of the stellar luminosity, $L_d/L_\star \sim 10^{-4}$ to 10^{-3}, typical of debris disks like HR 4796A (Low et al. 2005). The IR colors and spectral energy distributions of the latter group are consistent with predictions from cold debris disk models; sources with warmer dust may have terrestrial zone debris emission (see also C07b).

The MIPS data from h and χ Persei and other recently surveyed clusters yield a large sample of disks at 5–20 Myr, an age range critically important for understanding debris disk evolution and planet formation. This sample shows that debris disk emission rises from 5 to ~10 Myr, peaks at ~10–15 Myr, and then fades on a ~150 Myr timescale as t^{-1} (R05). Numerous statistical tests verify the observed trend. Debris production from ongoing planet formation explains the general time evolution of this emission (e.g., Kenyon & Bromley 2004b).

5.2. *Future Modeling Work: Explaining the Range of MIPS Excesses*

The debris disk models from Kenyon & Bromley (2004a) generally explain the peak excesses for sources in h and χ Per and other ~10–15 Myr old clusters. However, at a given age stars have a wide spread of IR excesses above and below the debris disk model predictions. The IR excesses far weaker than the model

predictions have several tenable explanations. Low-mass disks modeled in § 4 have weaker excesses. Disks in systems with binary companions close to the disk radius are probably disrupted quickly, although binaries with wider separations should have little effect, and very close separations may actually enhance infrared excesses (Bouwman et al. 2006; Trilling et al. 2007). Gas giant planets may also remove IR-emitting dust.

Reproducing the larger IR excesses ($K_s - [24] \gtrsim 4$–5) is more difficult. The debris disk model used in this paper yields a peak $K_s - [24] \sim 3.5$ (unreddened), but HR 4796A and several sources in h and χ Per and Sco-Cen have stronger excesses. More massive disks should yield stronger 24 μm excesses, but the disk mass cannot be increased indefinitely. A disk with mass $M_d \gtrsim 0.1 - 0.15\ M_\star$ would have been initially gravitationally unstable and would form a low-mass companion.

However, the debris disk status of one of these extreme cases, HR 4796A with $K_s - [24] \approx 5$, has been confirmed by extensive disk SED modeling (e.g., Augereau et al. 1999; Currie et al. 2003; Wahhaj et al. 2005) and strict gas mass upper limits of $\lesssim 1\ M_{\rm Jup}$ (Chen & Kamp 2004). There are several ways to account for these larger excesses.

For example, dynamical processes that allow small grains to be retained (which produce larger opacity) in rings like that observed for HR 4796A may explain the large-amplitude excesses in some debris disks (e.g., Klahr & Lin 2005; Takeuchi & Artymowicz 2001). Whether or not the strong excess sources in h and χ Per can be explained by such grain confinement mechanisms is the subject of future work.

5.3. *Comparison with Previous Spitzer Observations and Analysis of h and χ Persei from and Currie et al. (2007a) and (2007b)*

This paper completes the first study of the circumstellar disk population of pre–main-sequence stars in the massive double cluster, h and χ Persei. Together with C07a and (2007b, this work provides new constraints on the frequency, lifetimes, and evolutionary states of circumstellar disks in 10–15 Myr old stars. Here we summarize the main results and conclusion of these studies.

Spitzer data for h and χ Per provide clear evidence that the frequency of IR excess emission depends on wavelength and on the mass of the star (C07a; this paper, § 3). Stars in both clusters have a higher frequency of IR excess at longer wavelengths. Lower mass (1.4–2 $M_\odot$) stars have IR excesses more often than more massive ($\gtrsim 2\ M_\odot$) stars. Su et al. (2006) and Gorlova et al. (2007) derive similar results for other clusters. Taken together, these results are consistent with an inside-out clearing of dust from young circumstellar disks, as expected from theoretical models of planet formation (e.g., Kenyon & Bromley 2004b).

To compare the completeness level of the MIPS sample with the IRAC sample from C07a, we derive the fraction of IRAC sources with MIPS detections at each IRAC band. The IRAC survey has 90% completeness levels of ~14.5 at [4.5] and ~13.75 at [8]. The MIPS sample includes 87% (3%) of the IRAC sources with $[3.6] < 10$ ($[3.6] < 14.5$) and 88% (11%) of the IRAC sources with $[8] < 10$ ($[8] < 13.75$) within 25′ of either cluster center. Because the MIPS survey detects such a small percentage of the IRAC sources in C07a, we cannot analyze a statistically significant population of IRAC IR excess sources with MIPS detections. However, the MIPS sources yield interesting constraints on the Be star population in h and χ Per (§ 3.2) and demonstrate a clear peak in the time evolution of the 24 μm excess of debris disks (§ 4.).

Detailed analyses of the IRAC/MIPS colors and the broadband SEDs demonstrate that warm dust ($T \sim 240$–400 K) is visible in 11 cluster stars (C07b; this paper, § 3). The dust luminosities of 10 of these sources ($\sim 10^{-4}$ to $6 \times 10^{-3}\ L_\star$) suggest this emission arises from optically thin dust in a debris disk. The IR excesses of these sources—which comprise the majority of known warm debris disks (see Hines et al. 2006, Wyatt et al. 2007a, and Gorlova et al. 2007 for others)—are consistent with detailed calculations of terrestrial planet formation around ~2 $M_\odot$ stars (Kenyon & Bromley 2004a).

Most of the IRAC/MIPS IR excess sources show evidence for cooler dust with $T \sim 100$–200 K (this paper, §§ 3 and 4). Although the lack of 70 μm detections prevents us from deriving precise limits on the dust temperatures and luminosities, the *Spitzer* data suggest that most (perhaps all) of these sources are debris disks with SEDs similar to those observed in Sco-Cen, the TW Hya Association and other young clusters. (Chen et al. 2005b; Low et al. 2005). When combined with data from the literature, these data provide clear evidence for a rise in the magnitude of the IR excesses from debris disks from ~5 Myr to ~10–15 Myr followed by a fall from ~20 Myr onward.

Although theory provides a reasonably good first-order explanation for the time evolution of the IR excesses in $\gtrsim 1.4\ M_\odot$ stars, some aspects of the observations remain challenging. A large range of initial disk masses and binary companions can probably explain the large range in IR excesses at a given stellar age, but these explanations require further testing. Current theory does not explain the largest IR excesses observed in the 10–20 Myr old stars in h and χ Persei, Sco-Cen, and the TW Hya Association (specifically HR 4796A). Dynamical, radiative, and stochastic processes not included in the numerical calculations are possible solutions to this failure. Increasing the sample size of this extreme population would provide better constraints on these processes.

Finally, this survey has provided us with several interesting sources that warrant more detailed investigation. For instance, "source 5"—discussed here and in C07b)—is probably an extremely massive debris disk. With a fractional disk luminosity of $\sim 6 \times 10^{-3}$, its emission rivals that of HR 4796A, β Pic, and other massive, nearby debris disks. However, this source differs from these other sources in at least two important ways. First, its spectral type is later (F9) than most stars with massive debris disks. Second, it harbors far warmer dust ($T_d \sim 240$–330 K) than most massive debris disks like HR 4796A ($T_d \sim 110$ K; Low et al. 2005). This feature may make it more similar to the warm debris disk of HD 113766A in Sco-Cen, the second most luminous source in Sco-Cen shown in Figure 14 (Chen et al. 2005b), than to HR 4796A and β Pic.

Longer wavelength observations of this h and χ Per source (e.g., 30–100 μm) will better constrain its SED and thus its dust population(s). Mid-IR spectroscopy of this source may also provide clues to the chemical composition of its circumstellar dust to compare with models of cometary and asteroidal material (Lisse et al. 2008).

5.4. *Future Observations*

Future observations of h and χ Persei will provide stronger constraints on debris disk evolution and the possibilities for producing the wide range of debris disk emission. A deeper MIPS survey (approved for *Spitzer* cycle 4) of the double cluster will identify $\gtrsim$1000–2000 cluster sources with $[24] \lesssim 12.25$, the brightness of an 1.3 $M_\odot$ G9 (1.7 $M_\odot$ A8) star with a 3 (2) mag excess. This ~2 mag increase in sensitivity (~2260 s pixel^{-1} integration) should yield a larger sample of 24 μm excess sources, which will better

map out the distribution of mid-IR excesses during the primordial-to-debris disk transition. If the correlation of massive, high fractional luminosity disks with early A stars is purely a selection effect, then this deeper survey of h and χ Persei should reveal many massive debris disks around slightly later type stars like 'Source 5'. This survey will be complemented by a deeper IRAC survey (also approved for cycle 4) of the double cluster, which will identify h and χ Per sources with [5.8] ([8]) $\lesssim$15.9 (15.2), the brightness of a $\sim$0.8 $M_{\odot}$ M0 (1.0 $M_{\odot}$ K6) photosphere. The $\sim$1.5–2 mag increase in sensitivity ($\sim$120 spixel^{-1} integration vs. 20.8 spixel^{-1} from the C07a observations) will likely result in photometry for $\gtrsim$10,000–15,000 cluster stars through [8], assuming a typical cluster initial mass function (e.g., Miller & Scalo 1979). These two surveys will likely detect hundreds of debris disk (and perhaps transition disk) candidates and yield extremely strong constraints on evolution of dust in circumstellar disks from warm, inner regions (IRAC) to cooler regions (MIPS) at a critical age for planet formation.

Ground-based surveys of h and χ Persei may also provide important clues about the evolution of disks around young stars. For instance, the ability of binary companions to affect the mid-IR excesses from disks can also be tested. At $\sim$2.34 kpc, a binary system with separation of $\sim$100 AU (and thus able to truncate debris disks) has an angular separation of $\approx$0.04″. Such systems can be resolved by long-baseline interferometers such as the Keck Interferometer. Comparing the IR excesses from single and binary systems can then determine if weaker IR excess sources are binaries. A large-scale spectroscopic survey of all sources in h & χ Per brighter than $V \sim 21$ ($\gtrsim$10,000) is underway (T. Currie et al. 2007, in preparation). This survey will identify sources most likely to be h & χ Per members as well as those with strong Hα emission indicate of gas accretion. Preliminary work indicates that the population of accreting h and χ Per sources is nonnegligible ($\gtrsim$20–30; Currie et al. 2007c). Comparing the IR excesses of accreting sources with those that are not accreting may examine the role of residual circumstellar gas in affecting the mid-IR excesses from disks.

We thank the referee for a thorough review and suggestions which improved this manuscript. We also thank Michael Meyer, John Carpenter, Christine Chen, and Nadya Gorlova for useful discussions regarding debris disks in other clusters; Matt Ashby, Rob Gutermuth, and Anil Seth provided valuable advice regarding galaxy contamination. We acknowledge from the NASA Astrophysics Theory Program grant NAG5-13278, TPF grant NNG06GH25G, and the *Spitzer* GO program (Proposal 20132). T. C. is supported by a SAO predoctoral fellowship; Z. B. received support from Hungarian OTKA grants TS049872 and T049082. This work was partially supported by contract 1255094, issued by JPL/Caltech to the University of Arizona.

REFERENCES

Andrews, S., & Williams, J. 2005, ApJ, 631, 1134
Augereau, J. C., et al. 1999, A&A, 348, 557
Bai, L., et al. 2007, ApJ, 664, 181
Barden, S., et al. 1993, in ASP Conf. Ser., 37, Fiber Optics in Astronomy II, ed. P. M. Gray (San Francisco: ASP), 185
Barrado y Navascues, D., et al. 1999, ApJ, 520, L123
Berriman, G., et al. 1985, MNRAS, 217, 327
Bouwman, J., et al. 2006, ApJ, 653, L57
Bragg, A., & Kenyon, S. 2002, AJ, 124, 3289
———. 2005, AJ, 130, 134
Chambers, J. 2001, Icarus, 152, 205
Chen, C., & Kamp, I. 2004, ApJ, 602, 985
Chen, C., et al. 2005a, ApJ, 623, 493
———. 2005b, ApJ, 634, 1372
Currie, T., et al. 2003, in ASP Conf. Ser. 294, Scientific Frontiers in Research on Extrasolar Planets, ed. D. Deming & S. Seager (San Francisco: ASP), 265
———. 2007a, ApJ, 659, 599 (C07a)
———. 2007b, ApJ, 663, L105 (C07b)
———. 2007c, ApJ, 669, L33
Dachs, J., Kiehling, R., & Engels, D. 1988, A&A, 194, 167
Dahm, S., & Hillenbrand, L. 2007, AJ, 133, 2072
Decin, L., et al. 2003, ApJ, 598, 636
Dominik, C., & Decin, G. 2003, ApJ, 598, 626
Dominik, C., & Dullemond, C. 2005, A&A, 434, 971
Dougherty, S., et al. 1991, AJ, 102, 1753
———. 1994, A&A, 290, 609
Eisner, J., et al. 2006, ApJ, 637, L133
Fabricant, D., et al. 1998, PASP, 110, 79
———. 2005, PASP, 117, 1411
Gordon, K. D., et al. 2005, PASP, 117, 503
Gorlova, N., et al. 2006, ApJ, 649, 1028
———. 2007, ApJ, 670, 516
Habing, H. J., et al. 2001, A&A, 365, 545
Haisch, K., Lada, E., & Lada, C. 2001, ApJ, 553, L153
Hartmann, L., et al. 2005, ApJ, 629, 881
Hayashi, C.,1981, Prog. Theor. Phys. Suppl., 70, 35
Hernandez, J., et al. 2006, ApJ, 652, 472
Hillenbrand, L. A. 1998, ApJ, 116, 1818
Hines, D., et al. 2006, ApJ, 638, 1070
Kalas, P. 1998, Earth Moon Planets, 81, 27
Kenyon, S., & Bromley, B. 2002, ApJ, 577, L35
———. 2004a, ApJ, 602, L133
———. 2004b, AJ, 127, 513
———. 2006, AJ, 131, 1837
Kenyon, S., & Hartmann, L. 1987, ApJ, 323, 714
———. 1995, ApJS, 101, 117
Klahr, H., & Lin, D. N. C. 2005, ApJ, 632, 1113
Lada, C., et al. 2006, AJ, 131, 1574
Lisse, C., et al. 2008, ApJ, in press (arXiv: 0710.0839)
Low, F., et al. 2005, ApJ, 631, 1170
Indebetouw, R., et al. 2005, ApJ, 619, 931
Mathis, J. 1990, ARA&A, 28, 37
Mauche, C., et al. 1997, ApJ, 477, 832
Meyer, M., et al. 2007, in Protostars and Planets V, ed. B. Reipurth and, D. Jewitt (Tucson: Univ. Arizona Press), 573
McSwain, M., & Gies, D. 2005, ApJS, 161, 118
Miller, G., & Scalo, J. 1979, ApJS, 41, 513
Oosterhoff, P. Th. 1937 Ann, Sternw. Leiden, 17, 1
Ortega, V. G., et al. 2002, ApJ, 575, L75
Papovich, C., et al. 2004, ApJS, 154, 70
Rieke, G., et al. 2005, ApJ, 620, 1010 (R05)
Siess, L., et al. 2000, A&A, 358, 593
Sicilia-Aguilar, A., et al. 2005, AJ, 130, 188
———. 2006, ApJ, 638, 897
Slesnick, C., et al. 2002, ApJ, 576, 880
Strom, S., & Wolff, S. 2005, in Star Formation in the Era of Three Great Observatories (Cambridge: Harvard), http://cxc.harvard.edu/stars05/agenda/program.html
Su, K., et al. 2006, ApJ, 653, 675
Takuechi, T., & Artymowicz, P. 2001, ApJ, 557, 990
Trilling, D., et al. 2007, ApJ, 658, 1289
Wahhaj, Z., Koerner, D. W., & Sargent, A. I. 2007, ApJ, 661, 368
Wahhaj, Z., et al. 2005, ApJ, 618, 385
Weidenschilling, S. J. 1997, Icarus, 127, 290
Wetherill, G., & Stewart, G. 1993, Icarus, 106, 190
White, R., & Basri, G. 2003, ApJ, 582, 1109
Woolf, N. J., Stein, W. A., & Strittmatter, P. A. 1970, A&A, 9, 252
Wyatt, M., et al. 2007a, ApJ, 658, 569
———. 2007b, ApJ, 663, 365
Zuckerman, B., et al. 2001, ApJ, 562, L87